AFOSR-TR- 79-1146

LEVEL II

October 10, 1979

Final Report

AFOSR Contract No. F49620-77-C-0123
SRI Project No. PYU (350)-6687
Reporting Period: 15 August 1977 through
15 August 1979

CONTRIBUTION OF SURFACE CATALYSIS AND GAS PHASE REACTION TO CATALYTIC COMBUSTOR PERFORMANCE

Participating Personnel: C. M. Ablow, S. Schechter, H. Wise, and B. J. Wood

Approved:

R. W. Bartlett, Director
Materials Research Laboratory

P. J. Jorgensen, Vice President
Physical and Life Sciences Divisions

SRI International
333 Ravenswood Ave. • Menlo Park, California 94025
(415) 326-6200 • Cable: SRI INTL MPK • TWX: 910-373-1246

SECURITY CLASSIFICATION OF THIS PAGE (When Data Entered) Unclassified

REPORT DOCUMENTATION PAGE	READ INSTRUCTIONS BEFORE COMPLETING FORM
1. REPORT NUMBER AFOSR-TR-79-1146	2. GOVT ACCESSION NO.	3. RECIPIENT'S CATALOG NUMBER 9
4. TITLE (and Subtitle) CONTRIBUTION OF SURFACE CATALYSIS AND GAS PHASE REACTION TO CATALYTIC COMBUSTOR PERFORMANCE	5. TYPE OF REPORT & PERIOD COVERED FINAL report Aug 77 - Aug 79
	6. PERFORMING ORG. REPORT NUMBER SRI Project No PYU 5502-6687
7. AUTHOR(s) C. M. ABLOW, B. J. WOOD S. SCHECHTER H. WISE	8. CONTRACT OR GRANT NUMBER(s) F49620-77-C-0123
9. PERFORMING ORGANIZATION NAME AND ADDRESS SRI INTERNATIONAL 333 RAVENSWOOD AVE MENLO PARK, CA 94025	10. PROGRAM ELEMENT, PROJECT, TASK AREA & WORK UNIT NUMBERS 2303A2 61102F
11. CONTROLLING OFFICE NAME AND ADDRESS AIR FORCE OFFICE OF SCIENTIFIC RESEARCH/NA BLDG 410 BOLLING AIR FORCE BASE, D C 20332	12. REPORT DATE Oct 79 13. NUMBER OF PAGES 79
14. MONITORING AGENCY NAME & ADDRESS (if different from Controlling Office)	15. SECURITY CLASS. (of this report) UNCLASSIFIED 15a. DECLASSIFICATION/DOWNGRADING SCHEDULE

16. DISTRIBUTION STATEMENT (of this Report)

Approved for public release; distribution unlimited.

17. DISTRIBUTION STATEMENT (of the abstract entered in Block 20, if different from Report)

18. SUPPLEMENTARY NOTES

19. KEY WORDS (Continue on reverse side if necessary and identify by block number)

CATALYTIC COMBUSTION
CATALYTIC FLAME HOLDER
MONOLITH COMBUSTOR
HETEROGENEOUS COMBUSTION
HOMOGENEOUS COMBUSTION
TRANSITION FROM KINETICS TO DIFFUSION CONTROL

20. ABSTRACT (Continue on reverse side if necessary and identify by block number)

Engineering studies with catalytic combustors in the main burner and afterburner of aircraft propulsion systems have been concerned with the attainment of high combustion efficiency and flame stabilization of fuel-air mixtures outside the conventional flammability limits. The development of such devices that will perform at optimum efficiency over a broad range of operating conditions requires a detailed understanding of the flow of a reactive gas through ducts with catalytic walls, in which both hetorogeneous (wall) and homogeneous (gas) chemical reaction kinetics can occur. Of special interest to our study is the evaluation of the

DD FORM 1 JAN 73 1473 EDITION OF 1 NOV 65 IS OBSOLETE

UNCLASSIFIED
SECURITY CLASSIFICATION OF THIS PAGE (When Data Entered)

410 281

relative contributions of surface-catalyzed and gas-phase reactions to the total heat release rate in a catalytic combustor over a range of operating variables that include gas flow velocity, catalyst temperature, surface reactivity, and fuel-air ratio. Two catalytic combustor systems were employed. One involved stagnation point boundary layer flow with a catalytically active flat surface, the other duct flow in a multichannel catalytic monolith. The experimental studies were supplemented by theoretical calculations of heat release rates and temperature profiles based on models appropriate to the geometry and fluid dynamics of each catalytic combustion system. The result of our studies with dilute propane-air gas mixture and platinum coated surfaces have demonstrated that in both combustor configurations the gas phase combustion can be initiated by the wall-catalyzed reaction. In stagnation-point flow the heat release due to the homogeneous reaction is significant at low gas velocities and high surface temperatures. In this region of predominant gas-phase reaction the temperature profile exhibits a maximum with respect to distance from the catalyst surface. In the miltichannel monolith combustor, the axial temperature profile inside a centrally-located duct is strongly affected by heat conduction. Results of the computational analysis provide valuable information on the effect of various parameters on the temperature and reaction distribution in a catalytic monolith including surface reaction rate, gas-phase reaction rate transport parameters, axial conductivity, and flow velocity. The temperature-profile characteristic observed experimentally correspond satisfactorily to those predicted by the model for the case of exothermic heat release by surface initiated gas-phase reaction. The report is divided into three sections: (1) "Catalytic Combustion in a Stagnation Point Boundary Layer" (2) "Combustion in a Monolithic Catalytic Combustor with Gas Phase Reaction" (3) "Numerical Analysis of Catalytic Monolith Combustion"

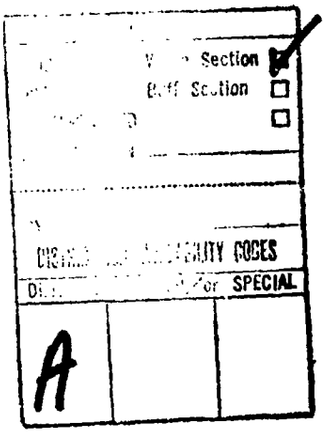

SUMMARY

Engineering studies with catalytic combustors in the main burner and afterburner of aircraft propulsion systems have been concerned with the attainment of high combustion efficiency and flame stabilization of fuel-air mixtures outside the conventional flammability limits. The development of such devices that will perform at optimum efficiency over a broad range of operating conditions requires a detailed understanding of the flow of a reactive gas through a duct with catalytic walls. Both heterogeneous (wall) and homogeneous (gas) chemical reaction kinetics as well as the fluid dynamics of laminar and turbulent flow need to be included in a model of the catalytic combustion system. To apply such a model it is necessary to establish the chemical kinetic parameters for the surface catalyzed and the gas-phase reactions that individually or jointly govern the heat release rates. Of special interest to our study is the evaluation of the relative contributions of surface-catalyzed and gas-phase reactions to the total heat release rate in a catalytic combustor over a range of operating variables that include gas flow velocity, catalyst temperature, surface reactivity, and fuel-air ratio.

In order to examine the respective roles of the various operating parameters in the combustion process, we studied two catalytic combustor systems. One involved stagnation point boundary layer flow with a catalytically active flat surface, the other duct flow in a multichannel catalytic monolith. The experimental studies were supplemented by theoretical calculations of heat release rates and temperature profiles based on models appropriate to the geometry and fluid dynamics of each catalytic combustion system.

The result of our studies with dilute propane-air gas mixture and platinum coated surfaces have demonstrated that in both combustor configurations the gas phase combustion can be initiated by the wall-catalyzed reaction. In stagnation-point flow the heat release due to

the homogeneous reaction is significant at low gas velocities and high surface temperatures. In this region of predominant gas-phase reaction the temperature profile exhibits a maximum with respect to distance from the catalyst surface. In the multichannel monolith combustor, the axial temperature profile inside a centrally-located duct is strongly affected by heat conduction. Under our experimental conditions the wall reaction is controlled by surface kinetics and not by mass transport of reactants to the wall. The location of the maximum temperature and its magnitude is a function of the mass flow rate of reactant through the combustor. These experimental data are interpreted with the aid of analytical modeling.

Results of the computational analysis provide valuable information on the effect of various parameters on the temperature and reactant distribution in a catalytic monolith, including surface reaction rate, gas-phase reaction rate, transport parameters, axial conductivity, and flow velocity. The temperature-profile characteristics observed experimentally correspond satisfactorily to those predicted by the model for the case of exothermic heat release by surface initiated gas-phase reaction. To attain high conversion efficiency of the fuel within a short length of catalyst, it is necessary to have high rates of surface-catalyzed and gas-phase reactions. Increasing the reactivity of the solid surface does not necessarily improve performance because of transition to a diffusion-limited mode of operation. Very high mass flux of the fuel-air mixture is detrimental to performance because it shortens the residence time and reduces the contribution of the homogeneous reaction.

The following sections of this report include a detailed description of the experiments and the results of our study. These sections are in the form of three Technical Reports entitled:

(1) "Catalytic Combustion in a Stagnation Point Boundary Layer"

(2) "Combustion in a Monolithic Catalytic Combustor with Gas Phase Reaction"

(3) "Numerical Analysis of Catalytic Monolith Combustion"

Technical Report No. 1

CATALYTIC COMBUSTION IN A STAGNATION POINT BOUNDARY LAYER

by

C. M. Ablow, S. Schechter, and H. Wise
SRI International
Menlo Park, California 94025

ABSTRACT

In order to examine the relative contribution of surface and gas phase reactions to the exothermic conversion of a fuel-air gas mixture flowing over a catalytic surface, we have carried out a theoretical and experimental study of catalytic combustion under stagnation point flow conditions. In the presence of exothermic surface reaction the theoretical model provides an analytical solution; in the presence of both reaction modes, homogeneous and heterogeneous, computer solutions were obtained for the total heat flux at the surface and the distribution of temperature, reactant, and product concentrations in the stagnation point boundary layer. Having available kinetic data on the platinum-catalyzed oxidation of propane and on the gas phase reaction between propane and air, we selected this chemical fuel system for experimental and theoretical study. Experimentally the flow of the propane-air mixture (1 vol% C_3H_8) was directed at a quartz plate whose surface was coated with thin strips of vacuum-deposited platinum, that served both as catalyst and resistance thermometer. During an experiment the temperature of each strip was maintained constant (± 5 K) by adjusting the electrical heat input as monitored by resistance measurements. By this procedure the heat released by exothermic reaction of the fuel-air mixture could be determined from the difference in electrical power required to keep each Pt stip at its original temperature. With the aid of the theoretical analysis we were able to compute the fractional contributions of catalytic and gas phase combustion to the total heat flux conducted to the catalytic surface. The relative contribution of each combustion

mode depended on catalyst activity, volumetric flow rate, and fuel/air ratio. Under our experimental conditions with transport limited surface reaction an increase in reactant flow rate enhances the surface-catalyzed contribution to the total heat release rate. The results obtained clearly indicate the conditions under which either combustion mode predominates.

I INTRODUCTION

The development of catalytic reactors for efficient combustion of various fuel-air mixtures is receiving considerable attention not only in pollution control but also in gas turbine thruster technology.[1,2] To a large measure the utility of catalytic combustors rests upon their ability to operate efficiently over a much wider range of fuel-air ratios than are imposed by the flammability limits of conventional gas burners. More recently the use of catalytic devices has been examined for NO_x-free combustion in gas turbine engines. Another interesting application in aircraft propulsion systems is flame stabilization in after burners by means of catalytic devices.[3,4]

While the selection of catalytic materials for efficient combustion has received considerable attention,[5] an analysis of the relative contribution of gas-phase reactions and surface-catalyzed processes to the performance of catalytic combustors over a range of operating conditions is made difficult by the complex interplay of fluid dynamics and reaction kinetics. The complexity of the theoretical analysis is lessened somewhat for the case of catalytic combustion with stagnation point flow conditions, because the flow field applicable to such a system is well understood.[6] The reactive gas mixture chosen for our studies was composed of propane-air since the global kinetics for the platinum-catalyzed surface reaction[7] and for the homogeneous gas-phase reaction[8] have been measured in our laboratory. The theoretical model for reactive stagnation point flow over a catalytic surface, the experimental measurements of heat release rate, and the interpretation of the results in terms of the model are presented in the following sections.

II THEORETICAL MODEL

In the theoretical modeling of the stagnation point flow catalytic reactor we consider two-dimensional, steady flow of a compressible, viscous fluid directed perpendicularly against a flat solid surface. The fluid is composed of a mixture of gaseous fuel and air that can undergo exothermic reaction in the gas phase and on the surface of the solid by catalytic reaction.

Cartesian coordinates (x,y) are introduced with origin at the stagnation point, the x-axis along the surface in an outflow direction, and the y-axis in the direction of the oncoming flow. The velocity components are u and v in the x and y directions, respectively. From the symmetry of the flow field, u will be an odd function of x, while the other dependent variables, v, density ρ, pressure p, temperature T, and fuel mass fraction Y, will be even functions of x. Near the y-axis

$$\begin{aligned} u &= x\, U_1(y) + \ldots \\ v &= V_0(y) + x^2 V_2(y) + \ldots \\ p &= p_0(y) + x^2\, p_2(y) + \ldots \end{aligned} \tag{1}$$

where the subscript is the same as the power of x. Subscripts 0 and 1 have been omitted below for brevity.

The equation for conservation of total mass,

$$\frac{\partial(\rho u)}{\partial x} + \frac{\partial(\rho v)}{\partial y} = 0 \quad ,$$

becomes to the lowest order in x,

$$\rho U + (\rho V)' = 0 \quad , \tag{2}$$

where the prime denotes differentiation with respect to y. The Navier-Stokes equations for conservation of momentum[9] reduce to

$$\rho(U^2 + VU') - (\mu U')' + (1/2)\, p_2 = 0 \quad , \tag{3}$$

$$\rho VV' - (4/3)\,(\mu V')' + p' = 0 \quad . \tag{4}$$

Equation (4) shows that pressure and velocity variations go together. For the slow flows of the present experiments, the pressure variation is a small fraction of its average value so that Equation (4) may be replaced by

$$p = \text{constant} \tag{5}$$

Variations of p_2 with y are similarly negligible, so that p_2 in Equation (3) is taken to be a constant.

The equation for conservation of fuel reads[10]

$$\rho\left(u\frac{\partial Y}{\partial x} + \frac{\partial Y}{\partial y}\right) - \frac{\partial}{\partial x}\left(\rho D\frac{\partial Y}{\partial x}\right) - \frac{\partial}{\partial y}\left(\rho D\frac{\partial Y}{\partial y}\right) = -R_G \tag{6}$$

where D is the diffusion coefficient and R_G is the rate of consumption of fuel by gas-phase reaction. Near the solid surface, derivatives with respect to x are negligibly smaller than those with respect to y. To the lowest order in x, one obtains

$$\rho VY' - (\rho DY')' = -R_G \quad . \tag{7}$$

Fuel-lean conditions are assumed so that variations in the concentrations of oxygen and inert species need not be considered.

If the contributions of mechanical work and viscous dissipation are neglected, energy conservation requires[9] for a steady state that heat production be balanced by convection and diffusion.

$$\rho\left[u\,\frac{\partial(CT)}{\partial x} + v\,\frac{\partial(CT)}{\partial y}\right] - \frac{\partial}{\partial x}\left(\lambda\frac{\partial T}{\partial x}\right) - \frac{\partial}{\partial y}\left(\lambda\frac{\partial T}{\partial y}\right) = (\Delta H)R_G \quad , \tag{8}$$

where C is the specific heat at constant pressure, λ the thermal

conductivity, and (ΔH) the heat of exothermic reaction. Near the stagnation point one obtains

$$\rho V(CT)' - (\lambda T')' = (\Delta H)\, R_G \qquad (9)$$

Since the pressure is constant by Equation (5) the perfect gas law gives

$$\rho T = \text{constant} \quad . \qquad (10)$$

At $y = \infty$, the variables have the known values

$$T = T_\infty \quad , \quad \rho = \rho_\infty \quad , \quad Y = Y_\infty \quad , \quad U = \beta \quad . \qquad (11)$$

Semiempirical expressions[11] determine β for given nozzle geometry and flow. Since $U' = U'' = 0$, Equation (3) gives

$$p_2 = -2\rho_\infty \beta^2 \quad . \qquad (12)$$

On the surface of the solid, at $y = 0$, the velocity vanishes, the temperature is prescribed, and the surface reaction is fed by diffusion:

$$U = V = 0 \quad , \quad T = T_S \quad , \quad D(\rho Y)' = R_S \quad , \qquad (13)$$

where R_S is the rate of consumption of fuel by the surface-catalyzed heterogeneous reaction.

Both reaction rates are taken to be of first order in the fuel concentration and, for these oxygen-rich conditions, of zero order in oxygen:

$$R_G = k_G \rho Y \quad , \quad R_S = k_S \rho Y$$

Nondimensionalization

Following the conventional boundary layer development[12] we introduce the nondimensional independent variable η and mass flux f, a function of η, by

$$\eta = y\sqrt{\rho_\infty \beta/\mu_\infty} \quad , \quad f = -\rho V/\sqrt{\rho_\infty \beta\, \mu_\infty} \quad . \tag{15}$$

Then by Equation (2)

$$\rho U = \rho_\infty \beta f_\eta \tag{16}$$

where the subscript η denotes differentiation. Equation (7) becomes

$$f\, Y_\eta + (1/\mu_\infty)\ (\rho D Y_\eta)_\eta = k_G\, \rho Y/\rho_\infty \beta \tag{17}$$

If the variation of C is neglected so that

$$CT' = (CT)' \quad , \tag{18}$$

Equation (8) may be written

$$fT_\eta + (1/\mu_\infty)\ (Le\rho D T_\eta)_\eta = -k_G\, (\Delta H)\rho Y/\rho_\infty \beta C \quad , \tag{19}$$

where Le is the Lewis number, $Le = \lambda/\rho CD$.

Elimination of y, U, and V from Equation (3) by means of Equations (12), (15) and (16) gives

$$f_\eta^2 - \rho f(f_\eta/\rho)_\eta - (\rho/\mu_\infty)\ [\mu(f_\eta/\rho)_\eta]_\eta - 1 = 0 \tag{20}$$

Boundary conditions on Equations (17), (19) and (20) as given in Equations (11) and (13) become

$$T = T_\infty \quad , \quad \rho = \rho_\infty \quad , \quad Y = Y_\infty \quad , \quad f_\eta = 1 \quad \text{at} \quad \eta = \infty \quad ,$$

$$f = f_\eta = 0 \quad , \quad T = T_S \quad , \quad (\rho Y)_\eta = (R_S/D)\ (\mu_\infty/\rho_\infty \beta)^{1/2}$$

$$\text{at} \quad \eta = 0 \quad . \tag{21}$$

Small Temperature Variation

If the fractional variation of temperature is small, the variations of ρ and μ in Equation (20) can be neglected to obtain an equation for f alone.

$$f_{\eta\eta\eta} + f f_{\eta\eta} - f_{\eta}^{2} + 1 = 0 \quad . \tag{22}$$

This equation with the boundary conditions on f in Equation (21) has been solved numerically by Hiemenz and others. The tabulated results[6,12] show that, at $\eta = 2.0$, f_{η} and u have reached 97% of their values at $\eta = \infty$. The boundary layer is therefore taken to extend from $\eta = 0$ to $\eta = 2.0$. A convenient analytic approximation to f that has two place accuracy throughout the boundary layer is given by

$$f = (a\eta^{2} + b\eta^{3})/(1 + c\eta + b\eta^{2})$$

$$a = 0.6047 \quad , \quad b = 0.2692 \quad , \quad c = 0.6338 \quad . \tag{23}$$

The indefinite integral of f is also needed:

$$\int f\, d\eta = \eta^{2}/2 + (a-c)\eta/b - [b + c(a-c)][\ln(1 + c\eta + b\eta^{2})]/2b^{2}$$

$$+ [2ab - c(3b + ac - c^{2})][\arctan\,(c + 2b\eta)/s]/b^{2}s \quad ,$$

$$s = (4b - c^{2})^{1/2} \tag{24}$$

When constant average values are taken for parameters D, C, and Le, Equations (17) and (19) reduce to

$$Y_{\eta\eta} + (Sc) f\, Y_{\eta} = (Sc)\, k_{G} Y/\beta \quad , \tag{25}$$

$$T_{\eta\eta} + (Pr) f\, T_{\eta} = -(Sc) k_G Y(\Delta H)/C\beta \quad , \tag{26}$$

where Sc is the Schmidt number, $Sc = \mu/\rho D$, and Pr is the Prandtl number, $Pr = Sc/Le$.

A. Catalytic Surface Combustion

In the absence of gas-phase reaction, $k_G = 0$, the equations have the solutions

$$Y = Y_S - (Y_S - Y_\infty)\, \varphi(\eta, Sc)$$

$$T = T_S - (T_S - T_\infty)\, \varphi(\eta, Pr) \tag{27}$$

where

$$\varphi(\eta, k) = \alpha(k) \int_o^{\eta} \exp\left[-k \int_o^{\eta} f d\eta\right] d\eta$$

and $\alpha(k)$ is the constant that makes $\varphi(\infty, k) = 1$. The tabulated[12] values of α are well fitted by

$$\alpha(k) = 0.570\, k^{0.4} \tag{28}$$

The values T_S, T_∞, and Y_∞ in Equation (27) are known; the value of Y_S is determined by the condition at the surface $\eta = 0$ as given in Equation (21):

$$Y_\eta = (k_S/D)\, (\mu/\rho\beta)^{1/2}\, Y$$

from which

$$Y_S = Y_\infty\, \alpha(Sc)/[\alpha(Sc) + (k_S/D)\, (\mu/\rho\beta)^{1/2}] \tag{29}$$

The heat flux from the solid surface by conduction to the fluid is

$$\dot{Q}_A = -\lambda \left.\frac{dT}{dy}\right|_{y=0}$$

$$= \lambda (T_S - T_\infty)\, \alpha(Pr) \sqrt{\rho\beta/\mu} \tag{30}$$

The heat flux to the catalyst surface by the exothermic, catalyzed surface reaction is

$$\dot{Q}_S = (\Delta H)\, D \frac{d(\rho Y)}{dy}\bigg|_{y=0}$$

$$= (\Delta H)\, \rho Y_\infty / [(1/k_S) + [1/D\, \alpha(Sc) \sqrt{\rho\beta/\mu}]] \qquad (31)$$

By regrouping the transport coefficients we can rewrite Equation (31) to read

$$\dot{Q}_S = m\, \dot{V}^{1/2} / [1 + (r/k_S)\, \dot{V}^{1/2}] \qquad (32)$$

where

$$r = D\, \alpha(Sc) \sqrt{\rho\beta_o/\mu}$$

$$m = r(\Delta H)\rho Y_\infty$$

and β_o is the semi-empirical constant of proportionality[11] between β and volumetric flow rate $\dot{V}$.

B. Catalytic Surface and Gas Phase Combustion

If reaction in the gas phase is included Equations (25) and (26) are not likely to have an analytical solution. They are solved here numerically for the temperature and fuel concentration. Functions and parameter values used in the calculations are given in Table 1. The coefficients D, ρ, and μ were taken as the average of their values of $T = T_\infty$ and for $T = T_S$.

For the propane/air system, the Schmidt number Sc is nearly temperature independent with numerical value unity. The Lewis number Le is also nearly temperature independent. If the Lewis number is also taken to be unity, Equation (25) can be replaced by the following linear combination of Equations (25) and (26):

$$J_{\eta\eta} + f\, J_\eta = 0 \qquad (33)$$

where

$$J = CT + (\Delta H)Y \quad . \qquad (34)$$

This equation has the solution

$$J = J_S - (J_S - J_\infty)\, \varphi(\eta, 1) \tag{35}$$

where function φ is defined for Equation (27).

Values of Y_∞ and T_∞ and T_S are given in Equation (21) so that J_∞ may be computed, while J_S is known only when a value is assumed for Y_S. In the overall numerical method we therefore assume a value for the constant Y_S, obtain function J from Equation (35), replace Y in Equation (26) by its expression as a function of J and T from Equation (34), and then solve the nonlinear differential Equation (26) for T as a function of η. Equation (34) then gives Y as a function of η so that the derivative Y_η can be computed at $\eta = 0$ and the wall boundary condition for Y in Equation (21) used to improve the assumed value of Y_S. After starting with the two extreme values $Y_S = 0$ and $Y_S = Y_\infty$ we obtained convergence in no more than three iterations with a secant method. In this method, the function of Y_S that is zero according to the wall boundary condition is taken to vary linearly between its two most recently computed values. The resulting linear equation is solved for the improved value of Y_S.

The differential equation to be solved for T is Equation (26) with Y replaced by its expression in terms of T and known function J as described above. The equation reads

$$T_{\eta\eta} + f\, T_\eta = k_G\, (CT - J)/C\beta \tag{36}$$

Multiplication by the function $F(\eta)$,

$$F(\eta) = \exp\left[\int_0^\eta f(\eta')\, d\eta'\right] \tag{37}$$

gives a differential equation in self-adjoint form

$$(F\, T_\eta)_\eta = G \quad , \quad G = k_G\, F(CT - J)/C\beta \tag{38}$$

The finite difference method of Marchuk and Babuska[13] has fourth-order accuracy, so that only a coarse mesh is needed. It produces a

tri-diagonal coefficient matrix from which a direct solution can be obtained. The method applies to linear equations in self-adjoint form and not to Equation (38) because k_G is a function of T. We describe the method for the linear equation

$$(FT_\eta)_\eta + ST = W \quad , \tag{39}$$

where F, S, and W are given functions of η or constants independent of T, and then adapt the method to solve nonlinear Equation (38).

Divide the interval of integration $\eta_o \le \eta \le \eta_\infty$ into uniform subintervals each of length h and let subscript i denote evaluation at a point $\eta_i = \eta_o + ih$: $F_i = F(\eta_i) = F(\eta_o + ih)$, and similarly for the other functions. Let a super bar denote the harmonic mean:

$$\bar{F}_i = 6/\left(F_{i-1/2}^{-1} + 4\,F_i^{-1} + F_{i+1/2}^{-1}\right) \quad .$$

Tridiagonal matrices B and M have for the three non-zero elements in their i-th rows $[B_{oi}, B_{1i}, B_{2i}]$ and $[M_{oi}, M_{1i}, M_{2i}]$ where, for i = 1, 2,..,n on a mesh with n interior points,

$$B_{oi} = [2 + (3F_{i-1/2}^{-1} - F_i^{-1})\,\bar{F}_{i-1/2}]/48$$

$$B_{1i} = [44 + (F_{i-1/2}^{-1} - 3F_i^{-1})\,\bar{F}_{i-1/2} + (F_{i+1/2}^{-1} - 3F_i^{-i})\bar{F}_{i+1/2}]/48$$

$$B_{2i} = [2 + (3F_{i+1/2}^{-1} - F_i^{-1})\,\bar{F}_{i+1/2}]/48$$

$$M_{oi} = -\bar{F}_{i-1/2} + h^2\,S_{i-1/2}\,B_{oi}$$

$$M_{1i} = \bar{F}_{i-1/2} + \bar{F}_{i+1/2} + h^2\,S_i\,B_{1i}$$

$$M_{2i} = -\bar{F}_{i+1/2} + h^2\,S_{i+1/2}\,B_{2i} \tag{40}$$

The finite difference approximation to the differential equation and boundary conditions is then

$$M\,\underline{T} = h^2\,B\,\underline{W} + \underline{C} \tag{41}$$

where $\underline{T}$ is the n-dimensional vector of unknown values of function T at the interior mesh points, $\underline{W}$ is the similar vector of known values of function W, and $\underline{C}$ is the vector with all zero entries except for $(h^2\,B_{o1}\,W_0 - M_{o1}\,T_0)$ as first entry and $(h^2\,B_{2n}\,W_{n+1} - M_{2n}\,T_{n+1})$ for n-th. Since the matrix M is tridiagonal, symmetric and generally non-singular, Equation (41) can be readily solved for T by recursion. The truncation error is of the order h^4, which allows for a smaller number of mesh points than more conventional difference methods. We tested this method over the interval $0 \le \eta \le 2$ with $f(\eta) = 2\eta$, which, for $k_G = 0$ and appropriate boundary conditions, yields the error function. The solution calculated with n = 31 was accurate at $\eta = 1$ to six decimal places.

For Equation (38), the nonlinear equation of physical interest here, Newton's method provides a linear differential equation for δ, the difference between the present guess T^o at the unknown function T and its generally more correct value $T^o + \delta$.

$$(F\,\delta_\eta)_\eta - G_T^o\,\delta = -(FT^o{}_\eta)_\eta + G^o \tag{42}$$

where G^o is G evaluated with $T = T^o$ and G_T is the partial derivative of G with respect to T. This is a linear differential equation for δ in the form of Equation (39) so that the finite difference method used for that equation can be applied here.

A theorem of Henrici[14] implies that the sequence of improved values of T, each obtained by Newton's method, will converge to the desired solution if G_T is non-negative. Now

$$G_T = k_{G,T}\,F(CT - J)/C\beta + k_G F/\beta$$

$$= -k_{G,T}\,F(\Delta H)Y/C\beta + k_G\,F/\beta$$

In these expressions k_G is a positive rate constant that increases with temperature, so that $k_{G,T}$ is positive, and the other quantities appearing

are all positive so that the condition for convergence is that the ratio $k_{G,T}\ (\Delta H)Y/Ck_G$ be less than unity. However, the iterations did converge with the ratio of the order of ten. We took for the initial guess T^o, the solution to the linear equation obtained from Equation (38) by setting $k_G = 0$. The number of iterations required was rarely more than six to achieve five place accuracy in a solution to the discrete problem.

To check the accuracy of the solution we tested the code on the problem

$$u'' = 2\ \exp(u)/(\cos 1)^2$$

$$u = 0 \text{ at } \eta = \pm 1$$

with solution

$$u = 2\ \ln[\ (\cos 1)/\cos \eta]\quad .$$

The exact value of u at $\eta = 0$, $u = -1.231253$, was computed except for a 6 rather than a 3 in the last place. The calculation had 31 interior nodes, was started with $u^o = 0$, and converged in 5 iterations.

III RESULTS OF THEORETICAL ANALYSES

In the absence of gas-phase reaction the results of the theoretical analysis show an interesting relationship between the exothermic heat release rate at the surface and the parameters involving chemical kinetics and fluid dynamics. The rate of heat transfer to the catalytic surface for a given fuel-air mixture exhibits two regimes depending on the relative magnitude of the two terms in the denominators of Equations (31) and (32). For the term $D\,\alpha(Sc)\,(\rho\beta/\mu)^{1/2} \ll k_s$, as would prevail at low gas velocity impinging on the stagnation plate or with high rate constants for the surface catalyzed reaction, the exothermic reaction is controlled by diffusive and convective transport of reactants to the catalyst surface. Under these conditions the term containing r is small in Equation (32) so that the heat release rate becomes a linear function of the square root of the gas velocity. By contrast, at high convective flow the term is large, and the heat release is governed by surface reaction kinetics and is independent of the gas velocity.

We have carried out some calculations for the C_3H_8-air system under study, using the model with surface catalyzed reaction involving Pt as the catalyst. For this analysis we have evaluated the parameters appropriate to this reacting system and to the physical geometry of the stagnation point flow apparatus discussed in further detail in the following section. Using temperature-averaged transport coefficients and the measured reaction kinetics for Pt-catalyzed combustion of propane-air mixtures,[7] we are able to calculate on the basis of Equation (32) the heat release rate at the surface as a function of the propane concentration in the gas stream, the surface temperature of the catalyst, and the reactant flow velocity. The results shown in Table 2 are limited to the surface catalyzed reaction and do not include any contribution from gas-phase combustion. The two reaction regimes are clearly distinguishable by the use of parameters in the table. One involves the transport limited surface process at low gas velocities, i.e. when $V \ll (k_s/r)^2$. Under these conditions the heat release rate becomes

proportional to the square root of the volumetric flow rate of the reactant gas mixture, i.e., $\dot{Q}_S$ is a linear function of $\dot{V}^{1/2}$ with slope m, which is nearly independent of temperature. At higher gas flow rate, so that $\dot{V} \gg (k_S/r)^2$, the heat release rate is governed by reaction kinetics; $\dot{Q}_S$ equals $(m\ k_S/r)$ and is independent of $\dot{V}$.

When both gas-phase and surface reaction are present an entirely different pattern emerges. Based on the results of the numerical analysis we have evaluated the relative contribution of the surface reaction to the total heat release rate at the surface (Figure 1). At low surface temperature and high gas flows the preponderance of the surface reaction becomes quite apparent. For example, with a gas mixture containing 1 vol percent C_3H_8 and a flow rate of 10 liters/minute, we find that the heat release traverses from a predominant surface reaction at 650 K to a predominant gas-phase reaction at 950 K. Reduction of the rate constant for the surface reaction, by reducing the preexponential factor by three orders of magnitude, is shown to be accompanied by a decrease in the heterogeneous contribution to the overall heat release rate (Figure 1).

The temperature profiles in the stagnation point boundary layer offer some insight into the effect of the gas phase reaction on the temperature gradient near the surface. The temperature profile at high gas velocity is characteristic of the predominantly surface catalyzed reaction (curve A, Figure 2). At lower gas velocity (curve B) the temperature gradient at the surface changes from negative to positive, as the gas-phase reaction predominates. Similar trends prevail in the temperature profiles computed at the higher surface temperature, except that the gas phase reaction contributes to the heat received by the surface even at the highest reactant flow rate shown. The temperature gradient at the surface is markedly reduced from that seen at the lower surface temperature for the same gas flow rate.

Of further interest is the fuel concentration profile in the stagnation point boundary layer adjoining the catalytic surface. As

shown by the data plotted in Figure 3, the profile depends on the relative contribution of gas and surface reaction. At the lower gas velocity the fuel concentration is significantly reduced throughout the boundary layer. This result is to be expected, since the gas phase contribution to the heat release is much greater at the lower velocities (Figure 1).

IV EXPERIMENTAL DETAILS

The stagnation point flow reactor selected for our studies is shown schematically in Figure 4. A stream containing the propane-air gas mixture of the desired composition is directed in an upward direction toward the catalytic surface, composed of a quartz support plate (10.4 cm x 10 cm x 0.1 cm) onto which a series of 12 separate platinum strips have been deposited by vacuum evaporation of the metal.* Each individual strip of the metal film (0.4 cm x 10 cm) extends over the entire width of the quartz plate. In the central section the metal film over a distance of 8 cm has a thickness of 4×10^{-5} cm while near the two ends, over a distance of 1 cm, the film thickness is 12×10^{-5} cm. Each of these Pt strips, separated by a distance of 0.1 cm, serves as a catalytic surface and resistance thermometer. At the ends of each strip electrical contact is made to a DC power supply and electrical circuit for resistance measurement. First each strip is heated electrically in an inert gas stream to specified temperatures, as measured by a radiation thermometer (with proper emissivity correction, $\epsilon = 0.65$), and its electrical resistance recorded at each temperature. Because of the difference in film thickness the temperature in the central portion of the Pt strip effectively governs its resistance. Over 90% of the length of each strip the temperature was found to be uniform within $\pm$ 5 K, with a sharp temperature gradient at the juncture with the thicker film ends. The electrical power required to maintain this temperature is measured as a function of inert gas velocity impinging on the plate. Subsequently we determine the power required to keep each strip at the same temperature (resistance) in the presence of the fuel-air mixture impinging at the same total gas velocity. Because of exothermic reactions at the surface and in the gas phase, the difference in power requirement represents the energy

---

*We would like to thank Dr. R. W. Schefer of the Lawrence Berkeley Laboratory for preparing the catalyst coated quartz plate.

generated by the chemical reaction. Thus, our measurements were carried out at constant catalyst temperatures, but different gas velocities and fuel-air mixture ratios. The incoming gas temperature in this series of experiments was maintained at 293 ± 5 K. The gas entered through a duct of rectangular cross section (1 cm x 8 cm), separated from the plate by a distance of 0.65 cm. The duct was oriented parallel to the Pt strips. The central strip was located in the center of the nearly two dimensional stagnation-point flow. During an initial heating period in nitrogen of about 2 hours the film sintered, and subsequently exhibited little change in its electrical properties, as determined in a series of recalibrations of its electrical resistance as a function of temperature. The quartz/Pt catalyst plate was rigidly suspended inside a glass cylinder (15 cm in diameter) through which a slow stream of N_2 was passed to sweep away the reaction products.

V EXPERIMENTAL RESULTS

As might be expected, the highest rate of exothermic reaction occurred near the central Pt strips exposed to the stagnation point flow containing C_3H_8-air. As a result it was found expedient to monitor only the heat release rates on the three central strips, which were responsible for more than 90% of the heat released to the entire catalyst plate over which reactive gas was flowing. The results of two experiments carried out at different catalyst temperatures are shown in Figure 5 for a fuel-air gas mixture containing 1 vol% C_3H_8. Here we correlate the measured heat release rates to the square root of the volumetric flow rate of reactive gas, as suggested by the theoretical analysis. Over a range of catalyst temperatures the experimental results are summarized in Table 3 in terms of the ratio of the heat release rate to the square root of the volumetric flow rate. It is to be noted that with rising catalyst temperature the ratio grows, i.e. for a given volumetric flow rate the heat release rate increases. If we were dealing entirely with transport controlled surface reaction this ratio would tend to decline, as manifested by the theoretical data listed in Table 3 (column 4). However the combined contributions of surface and gas-phase reactions readily explain the experimental results (Table 3).

The theoretical data are derived from the model by setting up the heat balance equation for the central platinum strip. The power $\dot{Q}_W$ required per unit area to maintain the strip at a fixed temperature is given by

$$\dot{Q}_W = \dot{Q}_A + \dot{Q}_B - \dot{Q}_S$$

where $\dot{Q}_A$ is the heat conducted to the gas stream, $\dot{Q}_B$ is the heat lost to the surroundings by conduction through the quartz plate or in other ways, and $\dot{Q}_S$ is the heat generated by surface reaction. Theoretical expressions are given for $\dot{Q}_A$ and $\dot{Q}_S$ in Equations (30) and (31). Let

added subscript I denote the values for an inert gas stream and subscript F for a stream with fuel present. Then

$$\dot{Q}_{BI} = \dot{Q}_{BF} \quad \text{and} \quad \dot{Q}_{SI} = 0$$

so that

$$\dot{Q}_{WI} - \dot{Q}_{WF} = \dot{Q}_{AI} - \dot{Q}_{AF} + \dot{Q}_{SF} \tag{43}$$

This difference $\dot{Q}$,

$$\dot{Q} = \dot{Q}_{WI} - \dot{Q}_{WF} \tag{44}$$

is the heat release rate measured experimentally for the data points in the figures and computed theoretically for the entries in Table 3. Equations (30) and (31) show that

$$\dot{Q}_A - \dot{Q}_S = -\lambda \frac{dT}{dy} - (\Delta H)\, D \frac{d(\rho Y)}{dy} \quad \text{at} \quad y = 0.$$

Since $\lambda = \rho CD$ and variations of ρ are being neglected, this difference may be written

$$\dot{Q}_A - \dot{Q}_S = -(\lambda/C) \frac{d}{dy} [CT + (\Delta H)Y] \quad \text{at} \quad y = 0$$

or by Equation (34)

$$\dot{Q}_A - \dot{Q}_S = -(\lambda/C) \frac{dJ}{dy} \quad \text{at} \quad y = 0$$

so that

$$\dot{Q} = -(\lambda/C) \left(\frac{dJ_I}{dy} - \frac{dJ_F}{dy} \right) \quad \text{at} \quad y = 0 \tag{45}$$

In the model, function J as given by Equation (35) is influenced by reaction only through Y_S and Y_∞. For the data shown in Figure 5, Y_∞ is

independent of flow speed and temperature and, in the diffusion controlled regime prevailing, Y_S is always zero. Hence $(J_I - J_F)$ is a fixed function of η, and $\dot{Q}$ is proportional to $d\eta/dy$ or $V^{1/2}$ as shown in Figure 6. The theoretical calculations of the separate contributions of the gas and surface reactions to the total $\dot{Q}$ are also shown in Figure 6.

VI DISCUSSION

In this study we have been able to demonstrate the contribution of heterogeneous and homogeneous reactions to the combustion of fuel in a stagnation point flow reactor with a catalytic surface. The theoretical analysis clearly indicates the conditions under which either combustion mode predominates. At 650 K the surface-catalyzed reaction is the major component of the total heat-release rate (Figure 6) over nearly the entire range of fuel-air gas velocities. An entirely different pattern emerges at 850 K. At this temperature we note the gradual transition from gas-phase predominance to surface-controlled heat release. At a flow rate of 160 $cm^3 \cdot s^{-1}$ the heat release rates by homogeneous and heterogeneous reaction are equal. At higher flow rates the gas-phase contribution declines relative to the surface reaction. The general pattern emerging from this analysis bears some similarity to the numerical analysis of CO oxidation catalyzed by Pt in a monolith reactor.[15]

It is to be noted that in the heterogeneous regime in which the heat release rate is transport limited, a more active catalyst will not improve the heat release rate. Only at impingement gas velocities so high that the catalytic reaction limits the conversion rate will an improvement in catalyst activity be accompanied by an increase in the surface-kinetics controlled limit of the heat-release rate.

The heat release rate by catalytic surface reaction attains one half of its maximum value ($m\ k_s/r$) at the square root of the volumetric flow rate (k_s/r). These values are given in Table 2. The flow rates required are considerably higher than employed in our experimental studies. Thus, in order to attain high combustion efficiency at moderate volumetric flow rates of fuel-air it is necessary to promote gas-phase combustion.

In general, the heat release rates measured experimentally compare favorably with the values derived from our theoretical model when the contribution of both combustion modes, heterogeneous and homogeneous,

is taken into account. The theoretical ratio $\dot{Q}/\dot{V}^{1/2}$ is independent of temperature (Table 3). The analytical modeling suggests a suitable experimental approach to measure the contribution of gas phase reaction to the combustion process in stagnation point flow. The temperature profiles in the boundary layer near the catalytic surface exhibit marked differences in the presence of homogeneous reaction (Figure 3). Thus a detailed study of the temperature distributions at various volumetric flow rates of fuel-air and different catalyst temperatures would allow elucidation of the gas-phase kinetics and its contribution in the overall combustion process.

In conclusion, the work described provides detailed information on the contribution of surface-catalyzed and gas-phase reactions to the combustion of a fuel-air mixture in stagnation point boundary layer flow. To make the theoretical model more precise the restriction of the Lewis number to unity should be removed. Experimentally, temperature probing within the boundary layer would further strengthen our understanding of the interplay of homogeneous and heterogeneous reaction kinetics with the fluid dynamics near a catalytic surface.

REFERENCES

1. D. N. Anderson, NASA Tech. Memo. 73786, September 1977.

2. S. M. DeCorso, S. Mumford, R. Carruba, and R. Heck, ASME Paper 76-GT-4, March 1976.

3. T. J. Rosfjord, AIAA Paper 76-46, January 1976.

4. L. C. Angello and T. J. Rosfjord, in Proceedings Third Annual Workshop on Catalytic Combustion, Env. Prot. Agency 600/7-79-038, February 1979.

5. R. S. Yolles and H. Wise, "Catalytic Control of Automobile Exhaust Emissions" Critical Reviews in Environmental Control, Vol. 2, pp. 125-146 (1971).

6. H. Schlichting, Boundary Layer Theory, McGraw-Hill Publ. Co., New York (1968).

7. A. Schwartz, H. L. Holbrook, and H. Wise, J. Catal. 21, 199 (1971).

8. C. M. Abłow and H. Wise, Combustion and Flame 22, 23 (1974).

9. L. Howarth, Modern Developments in Fluid Dynamics--High Speed Flow, Oxford (1953).

10. F. A. Williams, Combustion Theory, Addison-Wesley Publ. Co., Reading Mass. (1965).

11. D. T. Chin and C. H. Tsang, "Mass Transfer to an Impinging Jet Electrode," J. Electrochem. Soc., V125, 1461-1470 (1978).

12. S. Goldstein, Modern Development in Fluid Dynamics, Oxford (1938).

13. G. Birkhoff and S. Gulati, "Optimal Few-Point Discretizations of Linear Source Problems" SIAM J. Numer. Anal. Vol. 11, pp. 720-728 (1974).

14. P. Henrici, Discrete Variable Methods in Ordinary Differential Equations, John Wiley and Sons, New York, Chapter 7, (1962).

15. B. K. Harrison and W. R. Ernst, Comb. Sci. and Techn. 19, 31 (1978).

16. T. R. Marrero and E. A. Mason, J. Phys. Chem. Ref. Data, Vol. 1, 3-118 (1972).

17. J. A. Dean, Lange's Handbook of Chemistry, McGraw-Hill Book Company, New York (1973).

Table 1

FUNCTIONS AND PARAMETER VALUES FOR
THEORETICAL CALCULATIONS

Quantity	Equation	Reference
$\beta_O = 3.44 \times 10^{-3}$ $(s^{-1}/cm^3 \cdot min^{-1})$	(32)	11
$\Delta H = 1.1 \times 10^{4}$ $(cal \cdot g^{-1})$	(8)	17
$k_S = 1.1 \times 10^{9} \exp(-17000/RT)$ $(cm \cdot s^{-1})$	(29)	7
$k_G = 1.7 \times 10^{13} \exp(-21000/RT)$ $(cm^3 \cdot s^{-1} \cdot mol^{-1})$	(17)	8
$\mu/\rho = 9.36 \times 10^{-6} T^{1.707}$ $(cm^2 \cdot s^{-1})$	(15)	12*
$D = 2.70 \times 10^{-5} T^{1.59}$ $(cm^2 \cdot s^{-1})$	(16)	16*
$C = 0.30$ $(cal \cdot g^{-1} \cdot K^{-1})$	(8)	17
$\rho T = 0.35$ $(g \cdot K \cdot cm^{-3})$	(10)	17*

*Fit to data for air.

*Value for CO_2.

Table 2

HEAT RELEASE COEFFICIENTS AND SURFACE REACTION RATE CONSTANT FOR Pt CATALYZED COMBUSTION OF PROPANE IN AIR IN THE ABSENCE OF GAS PHASE REACTION*

Catalyst Temperature (K)	$\frac{m/X_\infty}{\frac{cal \cdot cm^{-2} \cdot s^{-1}}{(cm^3 \cdot s^{-1})^{1/2}}}$ ‡	$\frac{r}{\frac{cm \cdot s^{-1}}{(cm^3 \cdot s^{-1})^{1/2}}}$	k_S $(cm \cdot s^{-1}) \times 10^{-3}$	$\frac{m\ k_S}{X_\infty\ r}$ $(cal \cdot cm^{-2} \cdot s^{-1}) \times 10^{-3}$	k_S/r $(cc \cdot s^{-1})^{1/2} \times 10^{-3}$
550	9.45	0.21	0.21	2.30	1.03
650	9.07	0.24	2.30	20.94	9.65
750	8.79	0.27	13.16	103.9	49.4
850	8.55	0.29	49.94	341.3	169.9
950	8.35	0.32	143.1	891.5	446.8

*Cf Equation (32) in text.

‡X_∞ represents the mole fraction of fuel in the feed stream.

Table 3

HEAT RELEASE RATES AT
VARIOUS CATALYST TEMPERATURES

C_3H_8 (vol%)	Catalyst Temperature (K)	$\dot{Q}/V$ $[(cal \cdot cm^{-2} \cdot s^{-1})/(cm^3 \cdot s^{-1})^{1/2}] \times 10^2$		
		Experimental	Theoretical (surface)	Theoretical (surface + gas)
1.0	650	2.00	1.72	2.48
	733	2.52	1.63	2.47
	850	2.80	1.55	2.41
0.5	733	0.98	0.81	1.21

LIST OF FIGURES

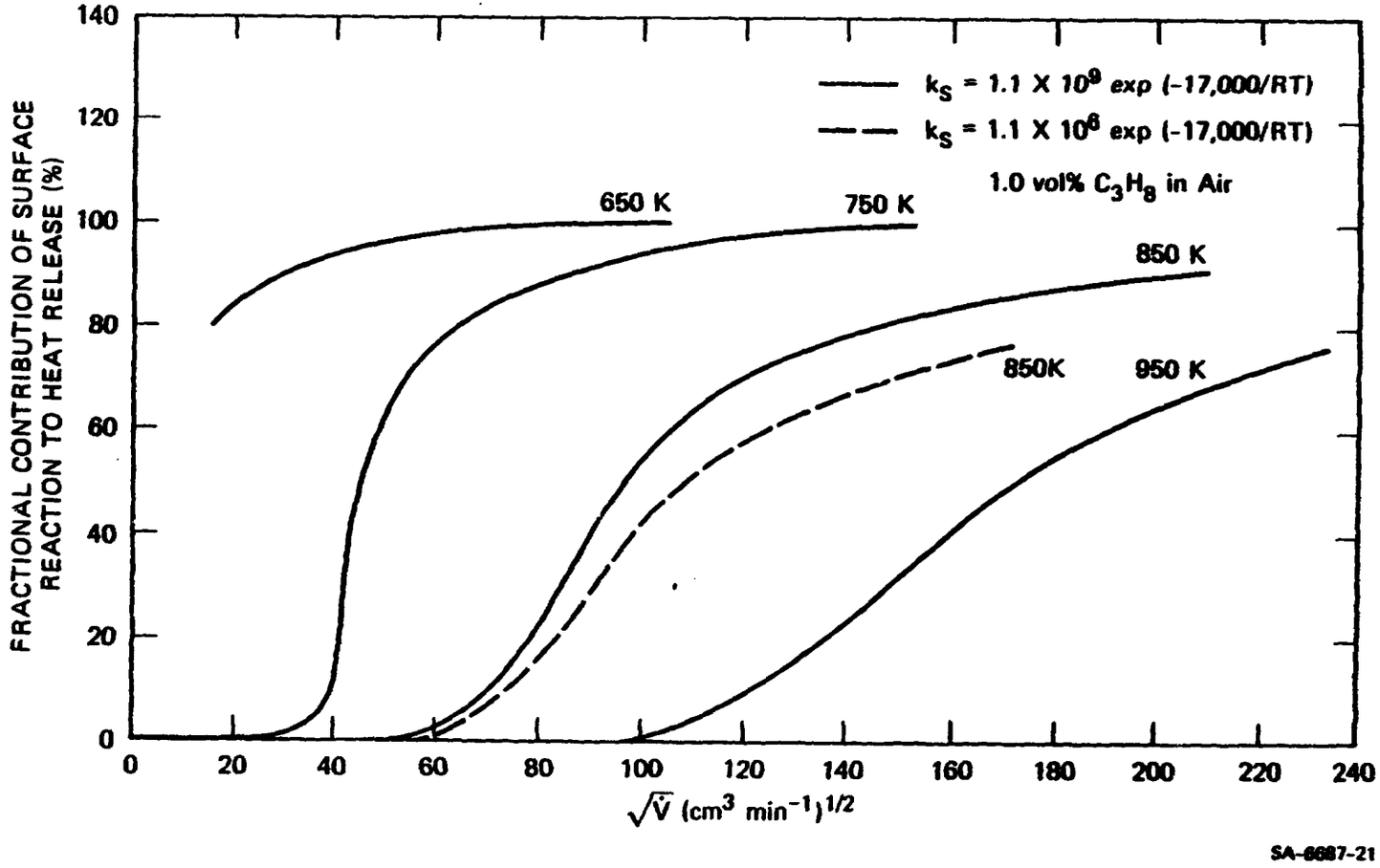

FIGURE 1 THEORETICAL FRACTIONAL CONTRIBUTION OF SURFACE CATALYZED REACTION TO TOTAL HEAT RELEASE RATE

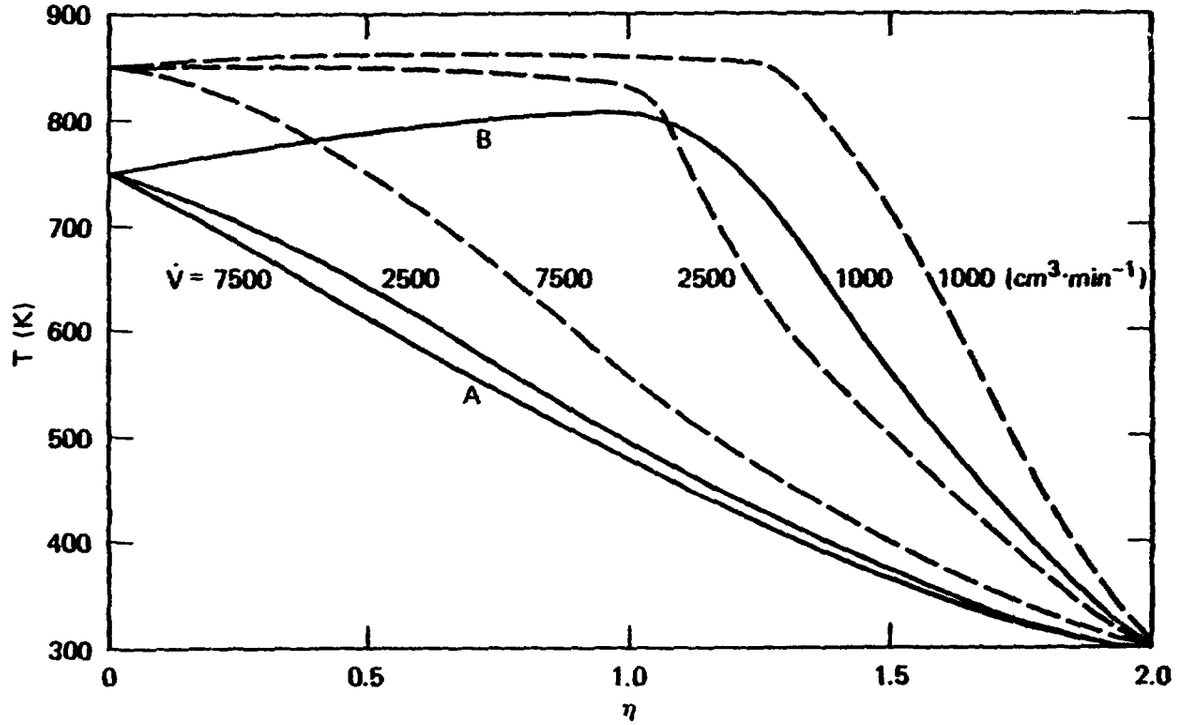

FIGURE 2 THEORETICAL TEMPERATURE PROFILES IN THE STAGNATION POINT BOUNDARY LAYER
(1 vol% C_3H_8 in air; —— T_S = 750 K; — — T_S = 850 K)

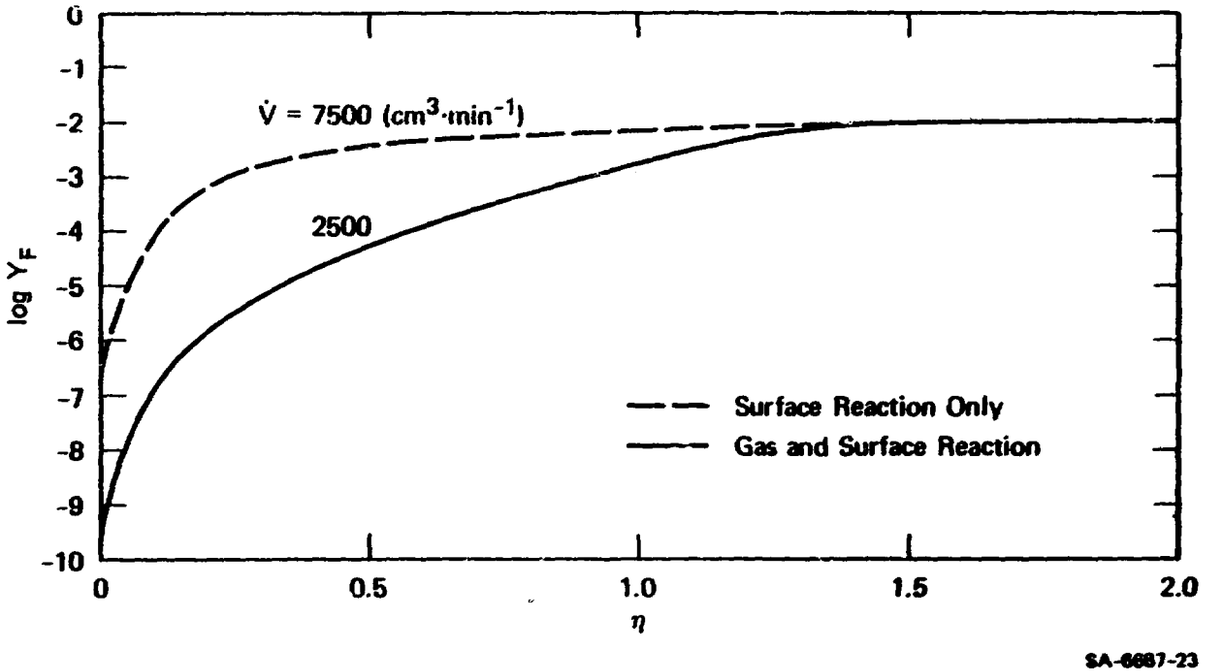

FIGURE 3 THEORETICAL FUEL FRACTION PROFILES IN THE STAGNATION POINT BOUNDARY LAYER (T_S = 850K)

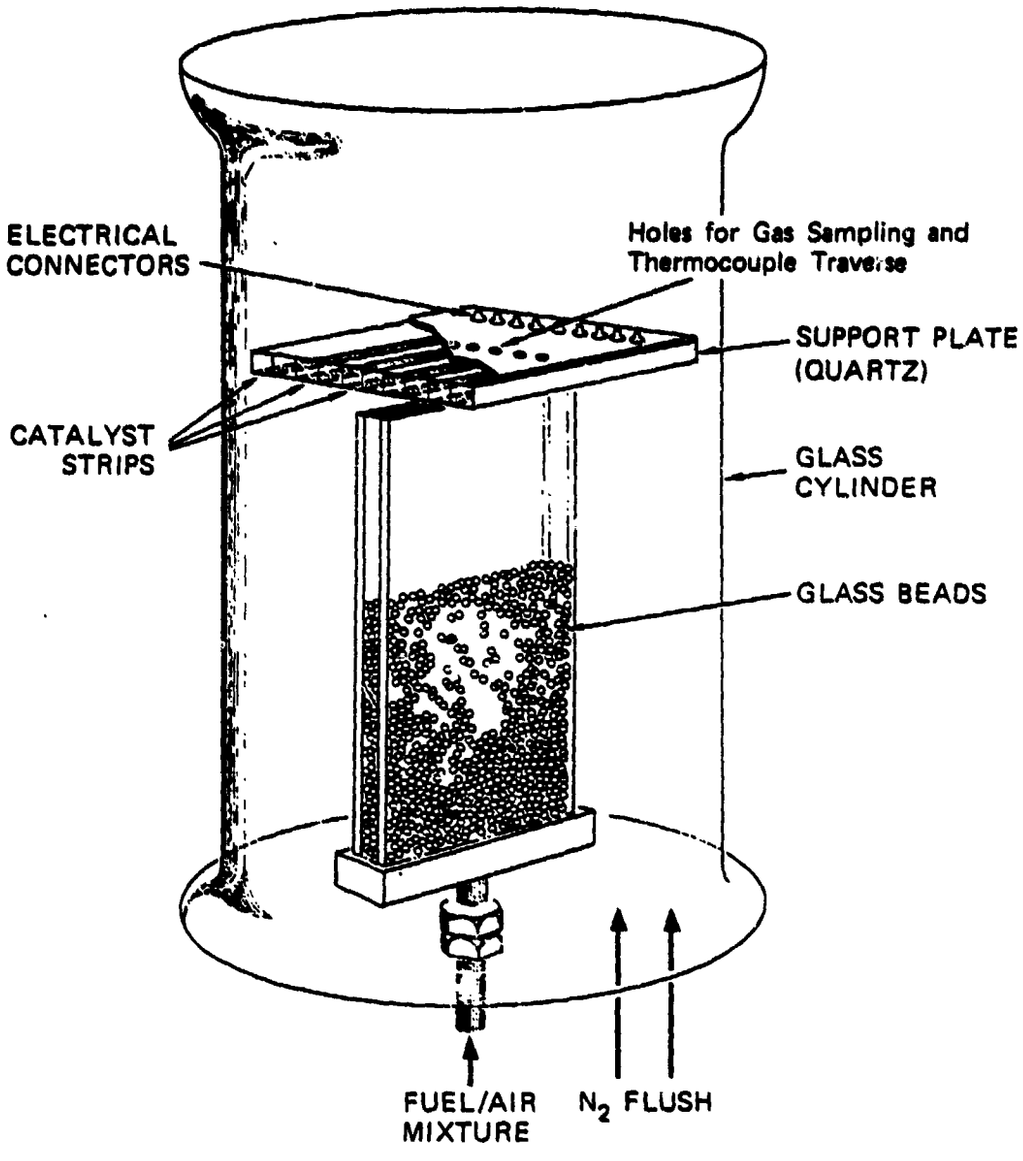

FIGURE 4 CATALYTIC COMBUSTOR WITH STAGNATION POINT FLOW

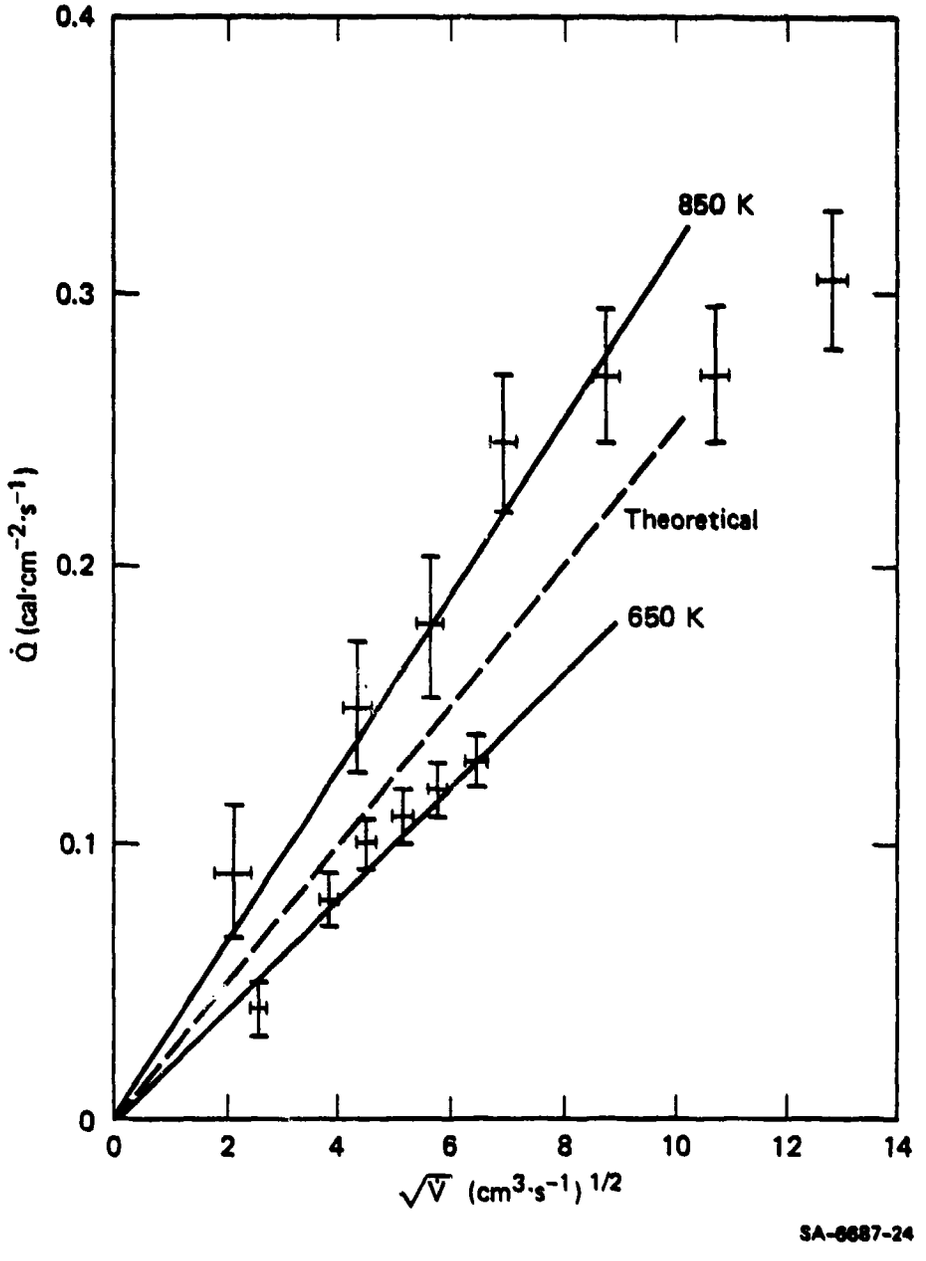

FIGURE 5 EXPERIMENTAL AND THEORETICAL RATES OF HEAT RELEASE TO THE CATALYTIC SURFACE (1 vol% C_3H_8 in air; Pt-catalyst plate)

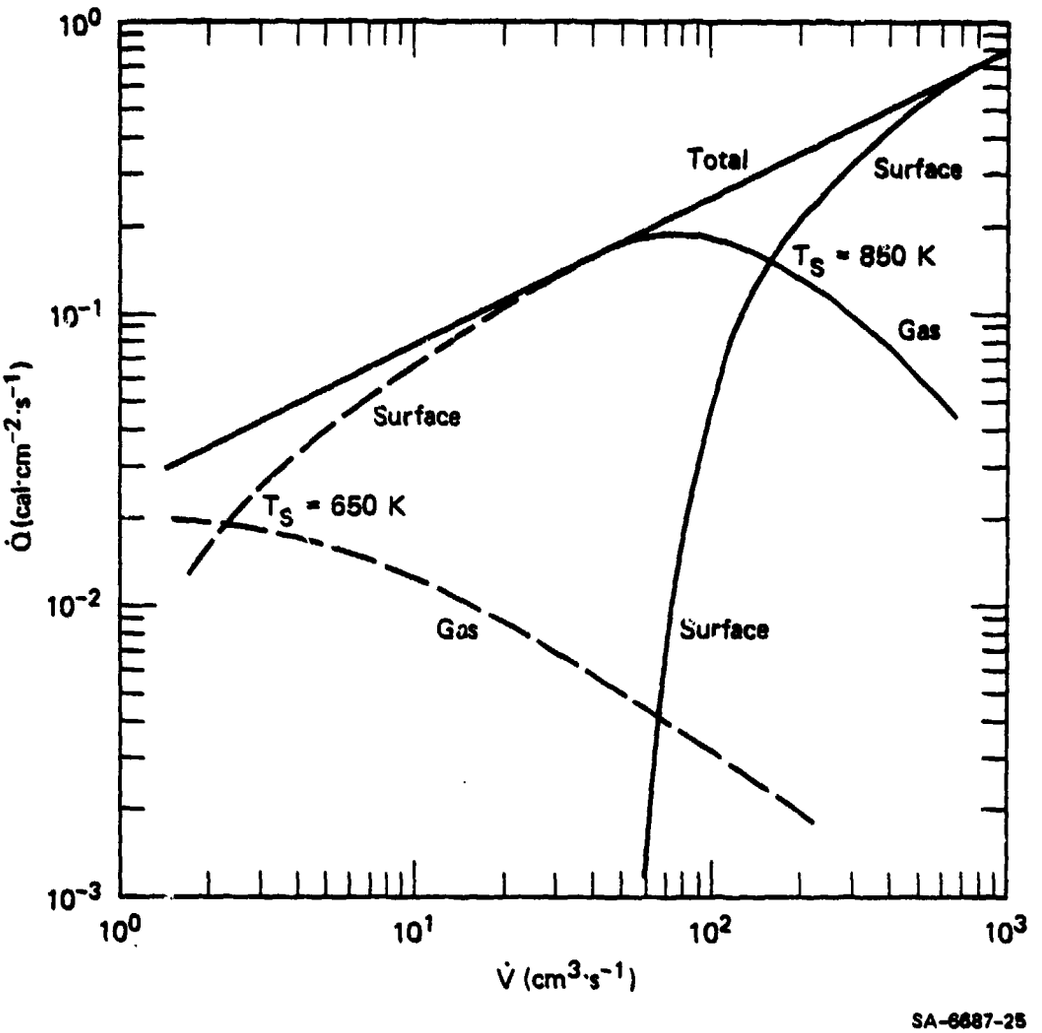

FIGURE 6 THEORETICAL HEAT RELEASE RATES BY HETEROGENOUS (SURFACE CATALYZED) AND HOMOGENEOUS (GAS PHASE) REACTIONS

Technical Report No. 2

COMBUSTION IN A MONOLITHIC CATALYTIC COMBUSTOR WITH GAS PHASE REACTION

by

C. M. Ablow, B. J. Wood, and H. Wise
SRI International
Menlo Park, California 94025

ABSTRACT

Experimental observations of the temperature distributions in a multichannel catalytic monolith, through which a mixture of propane and air is flowing, have been correlated qualitatively with a theoretical model. The correlation shows that gas-phase reaction is initiated by the catalyzed heterogeneous reaction, that the combustion is strongly influenced by heat conduction in the web of the solid, and that the surface reaction rate can be slow enough and the transport fast enough for chemical kinetic control of the process.

I INTRODUCTION

The design of a multichannel catalytic monolith for use as a flame holder[1] in aircraft afterburners will require accurate modeling of the initiation of gas-phase combustion by the heterogeneous reaction on the catalytically active surface. A steady-state, one-dimensional model that relates gas properties average at each cross section in a cylindrical catalyst channel to the local wall temperature and reaction rate by mass and heat transfer coefficients has been formulated with various degrees of approximation by several authors.[2-6] Based on such theoretical modeling, the predicted behavior of the system can be categorized into three distinct regimes,[6,7] dependent on the magnitudes of the system variables, such as gas velocity, temperature and fuel/air ratio. Briefly, these regimes comprise the following patterns: (1) a gradual increase of temperature with distance into the monolith; (2) a sharp temperature increase at the inlet or within the monolith; (3) a major contribution to total heat release by gas-phase reaction. Since the role played by gas-phase reactions inside the monolith is of special interest, we have carried out a series of experimental measurements designed to examine this regime in more detail. Their theoretical interpretation indicates that axial heat conduction by the solid monolith has a significant effect on combustor performance, even in the central channels of a large-diameter monolith where radial conduction is of lesser importance.

II EXPERIMENTAL STUDIES

In order to reduce heat losses by radial conduction and more closely approximate the adiabatic conditions in an interior channel of a catalytic monolith, the single-tube combustor used in earlier studies[5] was replaced by a multi-channel unit. The need for an array of channels with identical flows through them was clearly established by our success[6] in fitting to our model published data obtained with a monolith composed of several channels[5] after taking into account heat transfer to the surroundings.

The combustor is a 2.5 cm diameter core cut from a cordierite monolith.* It is 14 cm long and is completely coated with a platinum-impregnated alumina washcoat. Each channel has an open cross section 0.145 cm square (Figure 1) with a web thickness of 0.028 cm, and hydraulic radius R_H = 0.0363 cm. There is a minimum number of ten channels across any diameter of the core. Three of the channels were closed to gas flow by a plug of Sauereisen No. 1 cement at the upstream end of the combustor, as shown in Figure 1.

The catalytic monolith was situated in a 2.5 cm inside diameter fused quartz tube (Figure 2), and held in place with quartz retaining rings cemented to the tube. Propane-air and carbon monoxide-air mixtures were prepared by metering the gases through flow meters. The selected gas mixture entered the fused quartz tube and flowed through a 30 cm long section heated by an electric furnace. At the end of this preheat section the combustible gas mixture entered the combustor, which was also heated by an electric furnace. At the outlet of the catalytic monolith, the gases passed through a 15 cm long section of the fused quartz tube before being vented into a fume hood.

The axial and radial steady-state wall temperature profiles in the closed channels of the combuster were monitored by a set of three chromel-alumel thermocouples in 0.1 cm sheaths with exposed junctions. A fourth thermocouple was located in a central open channel to monitor the gas temperature. These thermocouples were attached to a single movable

*The material was kindly provided by Dr. L. L. Hegedus, General Motors Research Laboratories, Warren, Michigan.

fixture so that they could be moved axially as a unit to any desired cross section within the combustor. An additional thermocouple was fixed in the gas stream 1.5 cm ahead of the catalytic monolith.

Samples of gas from the feed stream and the product stream of the reactor were taken with gas-tight syringes. The samples were analyzed for propane, carbon monoxide, and carbon dioxide by injecting them into a gas chromatograph with Porapak T and 5A Molecular Sieve columns. Complete conversion of the fuel to CO_2 occurred during passage of the gas through the catalyst in al runs with $\dot{V} < 8\ \ell \cdot min^{-1}$. With $\dot{V} = 8\ \ell \cdot min^{-1}$, 96 vol% of the propane in the feed stream was found to be consumed.

Results of the experiments are presented in Figures 3 through 5. The radial profiles of the temperature at various axial distances from the inlet to the monolith (Figure 4) exhibit only small gradients. Hence, neglect of radial heat transfer in our analytical model represents a reasonable approximation of the experimental situation.

III THEORETICAL MODEL

A. Duct Flow Model*

The steady-state temperature and concentration distributions in each duct cross section are modeled by their average plug flow values in the gas phase, denoted by subscript G, and their values at the catalyst surface, subscript S. The heat balance in a cross section of the fluid reads

$$R_H \frac{d}{dx} (\rho_G v C_G T_G) = R_H \lambda_G \frac{d^2 T_G}{dx^2} - h_T(T_G - T_S) + R_H Q k_G \rho_G Y_G \qquad (1)$$

where, for the fuel-lean case, the nearly constant concentration of oxidizer is included in the reaction rate constant k_G. The heat transfer coefficient may be expressed in terms of either the Stanton or Nusselt numbers:

$$h_T = \rho_G v C_G St = (\lambda_G / 4R_H) Nu$$

The fuel mass balance in the fluid gives

$$R_H \frac{d}{dx} (\rho_G v Y_G) = R_H D \frac{d^2(\rho_G Y_G)}{dx^2} - h_M(\rho_G Y_G - \rho_S Y_S) - R_H k_G \rho_G Y_G \quad . \qquad (2)$$

The mass transfer coefficient h_M may be written in terms of the diffusion coefficient D of the fuel through the gas mixture and the Sherwood number Sh:

$$h_M = (D/4R_H) Sh \quad .$$

---

*The notation used in this paper is identical to that found in reference 6.

The fuel that diffuses to the surface of the catalyst is consumed by the reaction:

$$h_M(\rho_G Y_G - \rho_S Y_S) = k_S \rho_S Y_S \quad . \tag{3}$$

Finally, heat balance in the duct wall may be written as:

$$R_w \lambda_w \frac{d^3 T_S}{dx^2} + h_T(T_G - T_S) + Q k_S \rho_S Y_S = N_w h_T(T_S - T_E) \tag{4}$$

where N_w is the ratio of the heat transfer coefficients for exterior and interior temperature differences (subscripts E and S, respectively).

B. Governing Parameters

The governing parameters are found by a nondimensionalization of the equations. The dimensionless distance and temperature, ξ and τ, are taken to be

$$\xi = x \, St/R_H \, , \quad \tau = T/\Delta T_A \tag{5}$$

where the adiabatic temperature rise ΔT_A, is defined by

$$\Delta T_A = Q \, Y_{GO}/C_G$$

and a constant, uniform, average value is taken for the Stanton number, St, and for the other transport parameters, Nu, Sh, D, λ_G, etc.

Since $m = \rho_G v$ is a constant, Equation (1) may be divided by $mC_G(St)\Delta T_A$ to obtain

$$\tau'_G = \tau''_G/Pe_h - (\tau_G - \tau_S) + R_H \, Q k_G \rho_G Y_G/mC_G(St)\Delta T_A$$

where Pe_h the Peclet number for heat transfer in the stream, is defined by

$$Pe_h = R_H \, w \, C_G/\lambda_G St$$

and the primes denote differentiation with respect to ξ.

Introduction of the unburned fuel fraction y as a dependent variable, and use of the constant pressure relation, $\rho_G T_G$ = constant, reduce the equation to

$$\tau_G' = \tau_G''/Pe_h - (\tau_G - \tau_S) + \bar{k}_G \, y_G/\tau_G \quad ,$$

$$\bar{k}_G = k_G \, R_H \, \rho_{GO} T_{GO}/m(St)\Delta T_A \qquad (6)$$

Similar manipulation of Equation (2) results in

$$y_G' = y_G''/Pe_m - (Sh/Nu\ Le)[y_G - (\rho_S/\rho_G)y_S] - \bar{k}_G y_G/\tau_G$$

where Pe_m, the Peclet number for mass transfer, is defined by

$$Pe_m = R_H \, m/\rho_G D \, SE = LePe_h$$

and Le, the Lewis number, is defined by $Le = \lambda/\rho_G C_G D$. The analogy between heat and mass transfer, Sh = Nu, gives

$$y_G' = -y_G''/Pe_m - [y_G - (\rho_S/\rho_G)y_S]/(Le) - \bar{k}_G y_G/\tau_G \quad . \qquad (7)$$

Equation (3) reduces by the same method to

$$y_G - (\rho_S/\rho_G)y_S = (Le)\bar{k}_S y_S/\tau_S \quad ,$$

$$\bar{k}_S = k_S \rho_{GO} T_{GO}/m(St)\Delta T_A \qquad (8)$$

Finally Equation (4) becomes

$$\tau_S''/Pe_w + \tau_G - \tau_S$$

$$+ \bar{k}_S y_S/\tau_S = N_w(\tau_S - \tau_E) \qquad (9)$$

where Pe_w, the Peclet number giving the ratio of heat transfer between gas and solid to conduction in the solid wall, is defined by

$$Pe_w = R_H^2 \, h_T/R_w\lambda_s(St)^2 \quad .$$

The fuel fraction y_S at the catalytic surface can be eliminated from Equations (6), (7) and (9) by use of Equation (8). There remain the three following equations for the three variables y_G, τ_G, and τ_S:

$$-\tau_G''/Pe_h + \tau'_G = -(\tau_G - \tau_S) + \bar{k}_G \, y_G/\tau_G \qquad (10)$$

$$-y_G''/Pe_m + y'_g = -Fy_G - \bar{k}_G y_G/\tau_G \qquad (11)$$

$$\tau_S''/Pe_w + \tau_G - \tau_S + Fy_G = N_w(\tau_S - \tau_E) \quad ,$$

$$F = 1/(Le + \tau_G/k_S) \qquad (12)$$

Fraction F may be recognized as the factor that indicates the control of the heterogeneous, catalyzed reaction either by chemical kinetics, if $\bar{k}_S$ is small so that the second term dominates, or by diffusion, if $\bar{k}_S$ is large.[8]

This system of differential equations has a definite solution only if six boundary conditions are specified, such as the following. Entry values of gas composition and temperature determine y_G and τ_G at $\xi = 0$. Little heat is conducted through the ends of monolith duct walls so that one may take

$$\tau'_S = 0 \text{ at } \xi = 0 \text{ and } \xi = L \quad .$$

The fuel concentration and temperature in the gas stream at $\xi = L$, the exit from the monolith, will be continuous with conditions downstream. Precise conformance to these boundary conditions is not needed to apply the model qualitatively.

C. Application of Theoretical Model

Numerical values of the parameters were used to further simplify the model in the present application. Theoretical calculations[9] for the viscosity, conductivity, and specific heat of the pure gases N_2 and O_2 have been averaged to give the values presented in Table 1. The volumetric flow rate $\dot{V}$, an experimental variable, together with the density from the perfect gas law, determine the Reynolds number. The diffusivity of propane has been taken to be the same as that for carbon dioxide,[10] a gas of the same molecular weight. The calculated value of the Lewis number used in the model is near unity at all temperatures.

Experimental values of the flow rate $\dot{V}$ were no greater than 10 ℓ-min^{-1}. Hence, the Reynolds number is small and a laminar flow value for the Nusselt number[11] can be used to compute the Stanton numbers tabulated in Table 1.

The stream Peclet numbers for mass and heat are equal in a gas with Le = 1 and may be readily computed, as can the wall Peclet number when the wall conductivity is known. Our experimental determination of the wall conductivity is described in the Appendix. Since the wall Peclet numbers are two orders of magnitude smaller than the stream numbers and since these numbers appear as reciprocals, there is some justification for simplifying the equations of the model terms containing Pe_m and Pe_h.

Finally for a duct in the center of the monolith, surrounded by ducts containing similar reactive flows, radial heat transfer can be neglected. Then $N_w = 0$ and the equations of the model reduce to:

$$\tau'_G = -(\tau_G - \tau_S) + \bar{k}_G\, y_G/\tau_G \tag{13}$$

$$y'_G = -Fy_G - \bar{k}_G\, y_G/\tau_G \tag{14}$$

$$\tau_S''/Pe_w + \tau_G - \tau_S + Fy_G = 0 \quad . \tag{15}$$

A linear combination of the three equations,

$$\tau_S''/Pe_w - \tau_G' - y_G' = 0$$

can be integrated to give

$$\tau_S'/Pe_w = \tau_G + y_G - \tau_{GO} - 1 \tag{16}$$

Where the constant of integration has been evaluated by use of the boundary conditions at $\xi = 0$. Differential equations (13), (14), and (16) describe the simplified model. Boundary conditions for this third-order system may be taken to be

$$y_G = 1 \quad , \quad \tau_G = \tau_{GO} \quad \text{at} \quad \xi = 0$$

$$\tau_S' = 0 \qquad\qquad\qquad \text{at} \quad \xi = L$$

Since second derivative terms in y_G and τ_G have been dropped, no downstream boundary conditions are needed for these variables.

IV DISCUSSION

A. Effects of Flow Velocity on Temperature Distribution

The steady state wall-temperature profiles observed in the monolith at various flow rates (Figure 3) demonstrate a pronounced variation in shape as the inlet gas velocity is changed. Since the dimensionless distance variable ξ in the model (Equation 5) is proportional to $\dot{V}$, one expects temperature distributions at different speeds that are similar to one another, differing only in the distance scale. Some evidence of this effect is the experimental observation that the temperature maxima on the curves move away from the entry as the flow velocity is increased. However, the distance scale change does not explain the difference in the values of the temperature maxima or other differences in the shapes of the curves. These effects can only appear in the model through the Peclet parameters which are strongly velocity dependent. Thus heat conduction has an important effect on combustion. As the flow velocity tends to zero, so do Pe_w and the second derivative of τ_S [Equation (5)]. The model therefore predicts that the variation in the surface temperature with distance will become more nearly linear as the velocity decreases. The conclusion is supported by the data in Figure 3.

B. Contribution of Surface Reaction

Let $\tilde{F}$ be an average value for $(F + k_b/\tau_b)$ over a short distance from the inlet of the monolith. Then Equation (14) can be approximated by

$$y_G' = -\tilde{F}\, y_G \quad .$$

The solution of this equation that satisfies the initial condition $y_G = 1$ at $\xi = 0$ is

$$y_G = e^{-\tilde{F}\,\xi} .$$

Data in Figure 3 show that over the range of $\dot{V}$ employed, the surface temperature reaches a maximum some distance from the inlet to the monolith, indicative of a significant unburnt fuel fraction y_G in that region. Based on the model, this rise in temperature within the monolith can occur only if $\tilde{F}\,\xi_1 < 1$, where ξ_1 is the value of ξ for $x = 1$. Now

$$\xi_1 = St/R_H$$

$$\approx 2/(0.0363\ \dot{V})$$

based on the parameter values given in Table 1. Since $\dot{V} \leq 8$ ℓ/min, this gives $\xi_1 \geq 6$ and $\tilde{F} < 1/6$. Such small values of $\tilde{F}$ imply kinetically controlled conditions at the surface with $\bar{k}_S$ of the order of $\tau_G/6$. Apparently the catalytic surface activity is about three to four orders of magnitude less than that measured for Pt wire.[13]

C. Contribution of Gas Phase Reaction

The temperature difference $(T_S - T_G)$ plotted in Figure 5 is proportional to the dimensionless variable $\Delta = \tau_S - \tau_G$. Elimination of τ_G from the transport terms of Equation (10) gives

$$(\Delta'' - \tau_S'')/Pe_h + \tau_S' - \Delta' - \Delta = \bar{k}_G\, y_G/\tau_G \quad .$$

At the maximum value for the surface temperature, $\tau_S' = 0$ and τ_S'' is negative. The experimental results (cf. Figures 3 and 5) demonstrate also that Δ is near zero or negative, Δ' is negative and Δ'' positive, so that each term on the left of the equation is positive or zero. A positive gas reaction term is needed to balance the equation. Thus the model and the data correlate only if gas phase reaction is present at least in the vicinity of the temperature maxima in the catalyst.

If thermal conduction is neglected in both the gas and the wall, the model has an analytic solution. The solution exhibits for $Le \geq 1$ a surface temperature that increases monotonically with distance into the monolith, a condition irreconcilable with our experimental data.

In the following section (Technical Report No. 3) we apply numerical analysis to the model and compare the theoretical data with the experimental results.

V CONCLUSIONS

Our experimental multichannel catalytic combustor presents sufficiently well-defined conditions for theoretical modeling. Temperature profiles measured in the channels of the monolith correlate qualitatively with a model that distinguishes between temperatures or fuel fractions in the gas and at the catalytic surface.

The correlation indicates that axial heat conduction in the monolith walls has an important influence on the pattern of reaction in the ducts of the monolith, that the heterogeneous reaction on the catalytic surfaces of the monolith may be kinetically controlled, and that the catalyzed reaction of the duct walls can act to initiate gas-phase reaction.

REFERENCES

1. T. J. Rosfjord, "Catalytic Combustors for Gas Turbine Engines" AIAA paper 76-46.

2. L. C. Young and B. A. Finlayson, "Mathematical Models of the Monolith Catalytic Converter" AIChEJ, Vol. 22, pp. 331-353 (1976).

3. J. Votruba, J. Sinkul[illegible] Hlavace, and J. Skivanek "Heat and Mass Transfer in Monolithic Honeycomb Catalysts - I," Chem. Eng. Sci. Vol. 30, pp. 117-123 (1[illegible]).

4. R. H. Heck, J. Wei, J. R. K[illegible] "Mathematical Modeling of Monolithic Catalyts" AIChEJ, [illegible]. 22, pp. 477-484 (1976).

5. L. L. Hegedus, "Temperature Excursions in Catalytic Monoliths" AIChE J., Vol. 21, pp. 849-85[illegible] (1975).

6. C. M. Ablow and H. Wise, "Theoretical Analyses of Catalytic Combustion in a Monolith Reactor," Combustion Sci. Tech. (in press).

7. C. J. Pereira, J. J. Carberry, and A. Vosma, "Some Modeling and Simulation Aspects in Automotive Catalysts," Proc. Summer Computer Simulation Conference, Newport Beach, California (1978).

8. D. A. Franck-Kamenetskii, Diffusion and Heat Transfer in Chemical Kinetics, Plenum Press, New York (1969).

9. R. A. Sochla, "Estimated Viscosities and Thermal Conductivities of Gases at High Temperatures," NASA TR R-132, Lewis Research Center, Cleveland, Ohio (1961).

10. T. R. Manero and E. A. Mason, "Gaseous Diffusion Coefficients," J. Phys. Chem. Ref. Data, Vol. 1, 3-118 (1972).

11. S. Goldstein, Modern Developments in Fluid Dynamics, Oxford (1938).

12. Handbook of Chemistry and Physics, Chemical Rubber Publishing Company, Cleveland, Ohio (1956).

13. L. Hiam, H. Wise, S. Clarken, "Catalytic Oxidation of Hydrocarbons on Platinum," J. Catalysis, Vol. 10, pp. 272-276 (1968).

14. C. M. Ablow and H. Wise, "A Model Relating Extinction of the Opposed-Flow Diffusion Flame to Reaction Kinetics," Combustion and Flame, Vol. 22, pp. 23-34 (1974).

15. H. S. Carslaw and J. C. Jaeger, Conduction of Heat in Solids, Clarendon Press, Oxford (1959).

16. T. I. Barry, L. A. Lay, and R. Morrell, "Refractory Glass Ceramics," Proc. British Ceramic Soc., Vol. 22, 27 (1973).

Table 1

TRANSPORT PARAMETERS

Temperature (K)	$\mu_G \times 10^6$* (poise)	$\lambda_G \times 10^6$* ($cal \cdot cm^{-1} \cdot s^{-1} \cdot K^{-1}$)	C_G* ($cal \cdot g^{-1} \cdot K^{-1}$)	$Re/\dot{V}$ ($\ell \cdot min^{-1}$)	Le	$St \cdot \dot{V}$ ($\ell \cdot min^{-1}$)	$Pe_m/\dot{V}^2$ $(\ell \cdot min^{-1})^2$	$Pe_w/\dot{V}^2$ $(\ell \cdot min^{-1})^2$
500	262.4	93.9	0.24	3.17	1.01	1.96	0.28	0.0033
600	296.6	108.2	0.26	3.81	1.02	2.18	0.23	0.0031
700	328.3	122.3	0.26	2.54	1.03	2.39	0.19	0.0028
800	358.2	136.1	0.27	2.32	1.04	2.58	0.16	0.0027
900	386.5	149.6	0.27	2.15	1.04	2.77	0.14	0.0025
1000	413.8	162.8	0.27	2.01	1.05	2.95	0.12	0.0024
1100	444.4	175.8	0.28	1.87	1.05	3.12	0.11	0.0023
1200	466.4	188.5	0.29	1.78	1.06	3.28	0.10	0.0023
1300	491.3	200.7	0.29	1.69	1.06	3.44	0.09	0.0022

*Reference 9.

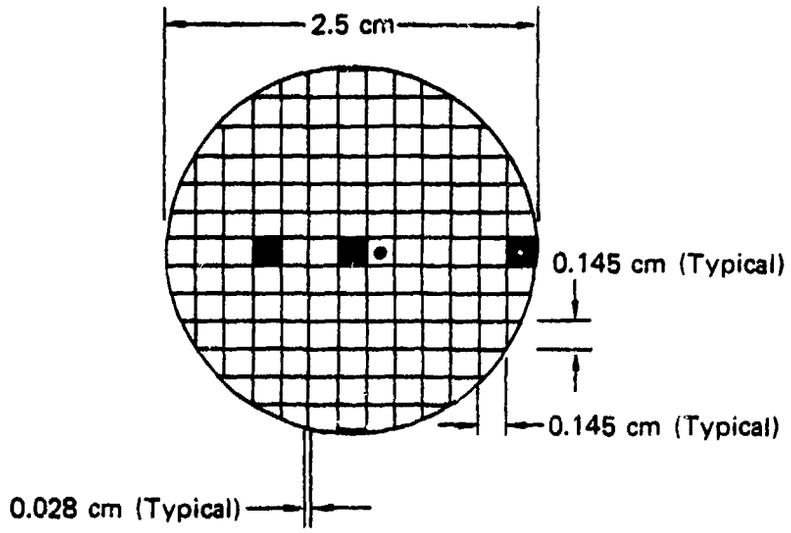

FIGURE 1 END VIEW OF MONOLITHIC CATALYTIC COMBUSTOR

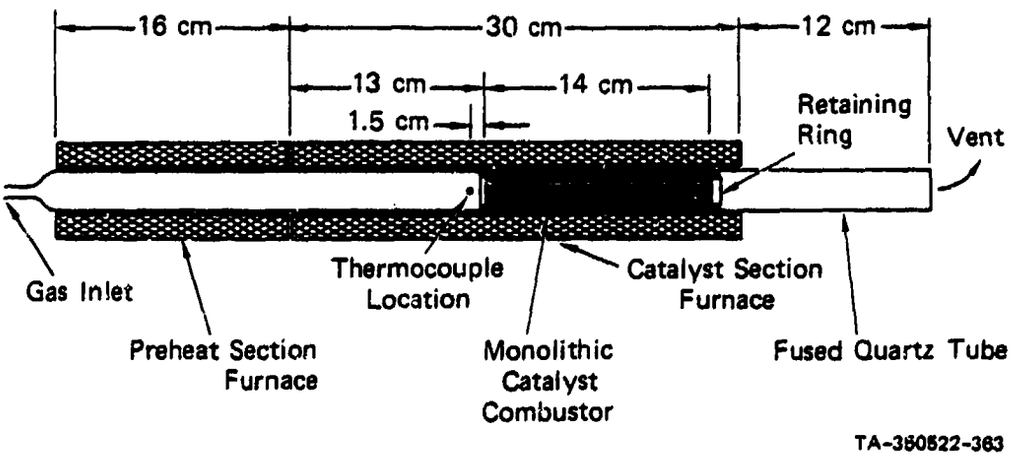

FIGURE 2 SCHEMATIC DIAGRAM OF EXPERIMENTAL APPARATUS

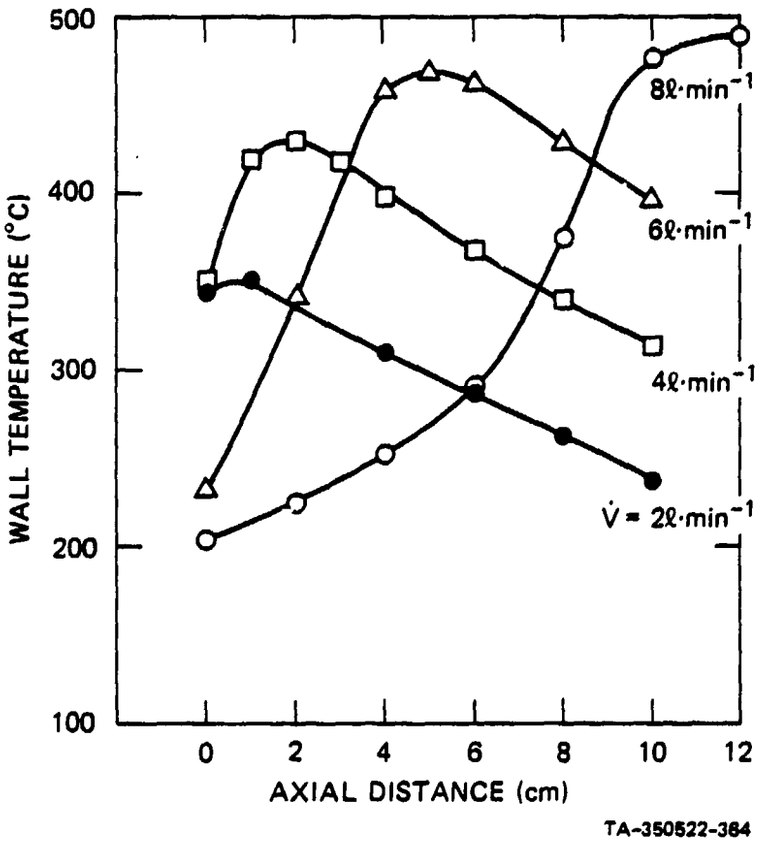

FIGURE 3 DEPENDENCE OF COMBUSTOR WALL TEMPERATURE ON AXIAL DISTANCE AND GAS VELOCITY

(Inlet Conditions: Propane/Air Ratio: 0.005; Gas Temp: 220 ± 10°C)

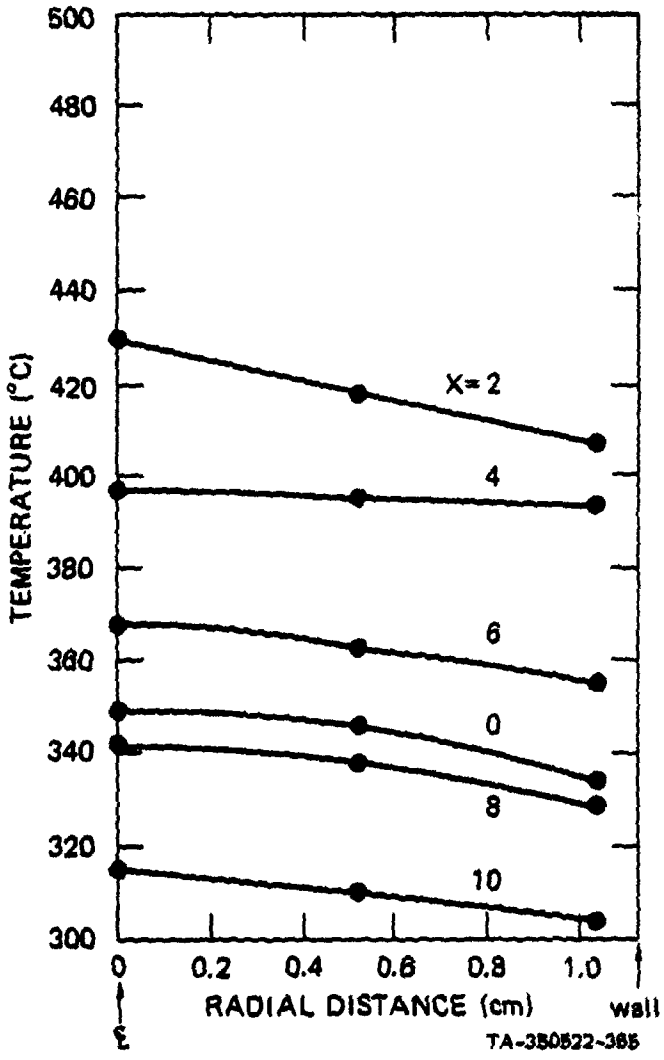

FIGURE 4 RADIAL TEMPERATURE PROFILES IN MONOLITHIC COMBUSTOR AT VARIOUS DISTANCES, X, FROM INLET

$\dot{V}$ = 4ℓ·min^{-1}, Inlet Conditions: Propane/Air = 0.005; Gas Temperature = 220°C.

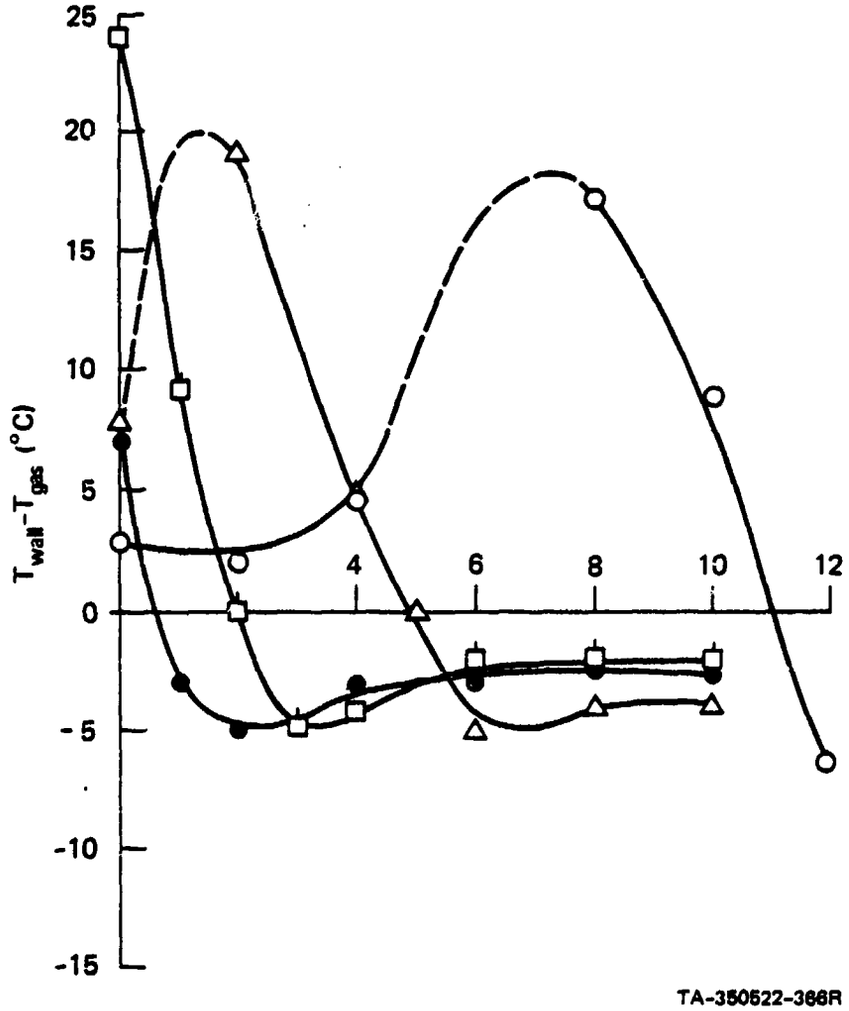

FIGURE 5 GAS-WALL TEMPERATURE DIFFERENTIAL AS A FUNCTION OF AXIAL DISTANCE AND GAS VELOCITY.

Initial conditions: Propane/Air = 0.005, Temperature = 220°C. Gas Velocity ($\ell \cdot min^{-1}$): ● 2; □ 4; △ 6; ○ 8.

Appendix

THERMAL CONDUCTIVITY OF THE MONOLITH

If the temperature of the surface of a semi-infinite slab is raised at a rate proportional to $t^{n/2}$, where t is the time and n is an integer, then the temperature rise within the slab of depth x is proportional to i^n erfc $(x/2\sqrt{\varkappa t})$ where $\varkappa$ is the thermal diffusivity in the slab and i^n erfc is the n-th integral of the complement of the error function.[15] One may show that the dominant term of an expansion of $\ln [i^n \text{ erfc } (u)]$, is $(-u^2)$ for any n as u becomes large.

To determine $\varkappa$, the thermal diffusivity, for the monolith core used in our experiments, the furnaces (Figure 2) were repositioned so that the juncture between them coincided with the location of the inlet end of the monolith. With the system at room temperature (298 K) and without any gas flow, the preheat section furnace (Figure 2) was energized, causing the temperature of the inlet face of the monolith to rise monotonocially with time. The face temperature, T_1, was monitored with a thermocouple situated at the mouth of the central blocked channel of the monolith. A second thermocouple, located in the adjacent channel exactly 3.8 cm from the inlet face, measured T_2 simultaneously. The temperatures recorded during the initial eight-minute interval are tabulated in Table A1.

A plot of $\ln(T_1 - 298)$ versus $\ln T$ shows that the front face temperature rose at a rate proportional to t^n with $n = 4.5$. Although n is not an integer, it may be expected that $\ln (T_2 - 298)$ will be a linear function of t^{-1} for small t. The data from t = 5 to 8 minutes does follow such a linear relation. From the slope one finds $\varkappa = 0.11$ $cm^2 \cdot s^{-1}$.

The average bulk density of the monolith, evaluated from the measured mass and dimensions of a cylindrical section is $\rho_w = 0.44$ $(g \cdot cm^{-3})$. This value is in reasonable agreement with published data[16] for the solid density of refractory glass ceramic material based on cordierite,

after correcting for a volumetric void ratio of 0.70. The specific heat for this material is $C_w = 0.21$ $(cal \cdot g^{-1} \cdot K^{-1})$.[16] Based on these parameters we find

$$\lambda_w = \chi \rho_w C_w = 0.010 \ (cal \cdot min^{-1} \cdot s^{-1} \cdot K^{-1}) \ .$$

Table A1

EARLY TIME MONOLITH TEMPERATURES CAUSED BY HEATING OF THE PREHEAT SECTION

Time t(min)	Temperature (K)	
	T_1 at x = 0	T_2 at x = 3.8 cm
0	298	298
1	-	-
2	303	-
3	315	-
4	330	-
5	351.5	299.5
6	378	301.5
7	405	304
8	435	307.5

Technical Report No. 3

NUMERICAL ANALYSIS OF CATALYTIC COMBUSTION

by

C. M. Ablow and H. Wise

ABSTRACT

A numerical analysis has been carried out of the contribution of surface-catalyzed and gas-phase reactions to the combustion of a dilute propane-air mixture in a catalytic monolith reactor containing highly dispersed platinum on its walls. The results obtained are in satisfactory agreement with the experimental measurements of the temperature profiles in the central duct of a multichannel monolith reactor. Specifically the numerical investigation demonstrates the effects of inlet gas velocity and inlet surface temperature on the location of the temperature maximum in the reactor and the monolith length required to attain a specified degree of conversion of fuel in the gas stream.

I. Introduction

Catalytic combustion in a tubular reactor has been modeled by several authors.[1-6] The one-dimensional model with slug flow appears to provide a suitable approximation when account is taken of:

- Reaction kinetics on the catalytic wall and in the gas stream.
- Convection of heat and mass by the stream
- Axial conduction of heat in the stream and in the tube wall
- Axial diffusion of reactants in the stream
- Radial diffusion of reactants and conduction of heat in the stream
- Radial conduction of heat through the tube wall to the exterior.

In order to obtain a better understanding of the interplay of the fluid dynamic and kinetic parameters and their relative importance in monolith combustion, we have carried out an analytic and numerical investigation of the solutions to a model applicable to the experimental studies presented in the preceding Technical Report No. 2. Again the contributions of surface-catalyzed and gas-phase reactions are of special interest in our analysis of monolith combustion.

II. The Model

For a specified gas mixture of fuel and oxidizer the adiabatic temperature rise ΔT_A is a suitable unit for normallizing the temperature. Nondimensional temperatures of the gas and the catalytic surface, τ_G and τ_S, are therefore defined by:

$$\tau_G = T_G/\Delta T_A \quad , \quad \tau_S = T_S/\Delta T_A$$

where T_G and T_S are the actual temperatures. The ratio y_G or y_S of the

fuel concentration Y_G or Y_S to the initial concentration in the gas stream Y_{GO} is a nondimensional fuel concentration variable, so that

$$y_G = Y_G/Y_{GO} \quad , \quad y_S = Y_S/Y_{GO} \quad .$$

The nondimensional axial distance ξ is taken to be

$$\xi = x\ St/R_H$$

where x is the actual distance from the monolith entry, R_H is the hydraulic radius of the duct, and St is the Stanton number, the ratio of heat convection to heat transfer between wall and stream. If follows that a temperature difference between two points, separated by one nondimensional unit on the stream axis, will produce the same heat flux as that difference would generate between two points in the same duct cross-section, one on the axis and one at the wall.

The steady state equations for heat and mass balance in the gas stream and at the duct wall can be combined[7] into the three following nondimensional differential equations:

$$\tau_G''/Pe_b - \tau_G' - (\tau_G - \tau_S) + \bar{k}_G\, y_G/\tau_G = 0 \quad , \tag{1}$$

$$y_G''/LePe_h - y_G' - Fy_G - k_G\, y_G/\tau_G = 0 \quad , \tag{2}$$

$$\tau_S''/Pe_W + \tau_G - \tau_S + Fy_G = N_W\,(\tau_S - \tau_E) \quad , \tag{3}$$

$$F = 1/(Le + \tau_G/\bar{k}_S) \quad ,$$

where the primes denote differentiation with respect to ξ, Le is the Lewis number (the ratio of heat conduction to fuel diffusion), Pe_h the Peclet number (the ratio of thermal convection to conduction in the gas stream), and Pe_W the mixed Peclet number (the ratio of thermal convection in the stream to conduction in the duct wall), constant N_W is the ratio of the heat transfer coefficients from the wall to the exterior.

The nondimensional kinetic rate constants for gas phase reaction $\bar{k}_G$ and surface reaction $\bar{k}_S$ are taken to be constant multiples of Arrhenius exponential functions of the temperature, an adequate approximation for fuel lean conditions (cf. Technical Report No. 2).

Because the monolith is of finite size the duct wall conducts no heat through X = 0 and X = L so that

$$\tau'_S = 0 \quad \text{at} \quad \xi = 0 \quad \text{and} \quad \xi = \xi_L \quad . \tag{4}$$

For a duct in the center of the multichannel monolith, radial heat transfer to the exterior is negligible, $N_W = 0$. Continuity with incoming and outgoing unconfined streams, in which radial heat transfer is also negligible, makes a reasonably accurate model of the monolith environment. As a result one obtains

$$\tau''_G/Pe_h - \tau'_G + \bar{k}_G\, y_G/\tau_G = 0 \tag{5}$$

$$y''_G/Le\ Pe_h - y'_G - \bar{k}_G\, y_G/\tau_G = 0 \tag{6}$$

valid for $\xi < 0$ or $\xi > \xi_L$, together with the boundary conditions

$$\tau_G = \tau_{GO} \quad , \quad y_G = 1 \quad \text{at} \quad \xi = -\infty$$

$$\tau'_G = y'_G = 0 \quad \text{at} \quad \xi = \infty$$

τ_G, τ'_G, y_G, and y'_G are continuous at

$$\xi = 0 \text{ and } \xi = \xi_L \tag{7}$$

In the next section we make further approximations and simplifications of the model by consideration of the relative magnitudes of the transport parameters.

III Application

In the experimental set-up of monolith combustion described in Technical Report No. 2, the configuration of the monolith was so designed as to reduce radial heat losses to a minimum for the centrally located ducts, as confirmed by the temperature measurements in a cross section of the monolith. With $N_W = 0$, the sum of Equations (1), (2), and (3) reads

$$(\tau''_G + y''_G/Le)/Pe_h + \tau''_S/Pe_W = \tau'_G + y'_G \quad .$$

This may be integrated to give

$$(\tau'_G + y'_G/Le)/Pe_h + \tau'_S/Pe_W = \tau_G + y_G - c \tag{4}$$

where c is a constant of integration. Based on the transport parameters listed in Table 1 one finds that Pe_h differs by two orders of magnitude from Pe_W. It is therefore reasonable to neglect the terms containing Pe_h in Equation (4). Also with further approximation we neglect these terms in Equations (1) and (2) to obtain the first order system

$$\tau'_G = \tau_S - \tau_G + \bar{k}_G\, y_G/\tau_G \tag{8}$$

$$y'_G = -(F + \bar{k}_G/\tau_G)y_G \tag{9}$$

$$\tau'_S = Pe_W\,(\tau_G + y_G - c) \tag{10}$$

The neglect of thermal and mass diffusion in the stream allows discontinuities of the diffusive flux at $\xi = 0$ and $\xi = \xi_L$ so that the boundary conditions can be simplified to

$$\tau_G = \tau_{GO} \quad , \quad y_G = 1 \quad , \quad \tau'_S = 0 \quad \text{at} \quad \xi = 0$$

$$\tau'_S = 0 \qquad\qquad\qquad\qquad\qquad\qquad \text{at} \quad \xi = \xi_L$$

The conditions at $\xi = 0$ show that

$$c = 1 + \tau_{GO} \quad .$$

Equations (8), (9), and (10) have been solved numerically by the use of a standard computer routine for solving initial-value problems. To use the routine one specifies a value for τ_S at $\xi = 0$. The correct τ_S has been chosen if the unused boundary conditions, $\tau'_S = 0$ at $\xi = \xi_L$, is found to be satisfied. However, the numerical solutions show the surface temperature increasing to a maximum and then falling with no leveling off to meet the downstream conditions. This behavior is probably true for linearized versions of the equations which have solutions for τ_S of the form

$$\tau_S = A + Be^{-b\xi} + Ce^{-c\xi} + De^{-d\xi}$$

where A, B, C, D, b, c, and d are real constants. The equation $\tau'_s = 0$ may then be written

$$bB + cC\, e^{(b-c)\xi} + dDe^{(b-d)\xi} = 0 \quad .$$

This equation, like a three-term polynomial, can have at most two roots. Thus τ'_S can be zero in at most two points. One of these has been fixed at $\xi = 0$. The other is at the maximum for τ_S. The downstream boundary condition cannot be satisfied in the linearized cases and probably not for the nonlinear equations.

Using the coefficients listed in Table 1, we have obtained numerical solutions for the axial temperature distribution in the catalytic duct wall as a function of the inlet surface temperature, τ_{SO} (Figure 1). It will be noted that at the fixed inlet gas temperature, the value of τ_{SO} has a pronounced effect on the temperature profile. Also a change in the surface reaction rate, brought about mathematically by reducing the preexponential coefficient by several orders of magnitude brings about a marked change in the location of the temperature maximum and its absolute value (Figure 2). At higher inlet gas velocities (V = 6 l/min)

the value of the inlet surface temperature has even a more pronounced effect on the temperature profile (Figure 3). At an inlet temperature T_{SO} slightly above the inlet gas temperature ($T_{GO} - T_{SO} = 1.5$ K) the surface reaction rate is too slow to cause significant heat release. At somewhat higher inlet surface temperatures a marked exothermic reaction is initiated. Under these conditions we observe that the maximum in the temperature profile moves toward the duct inlet as T_{SO} is increased. This effect of the inlet surface temperature on the location of the temperature maximum X_{max} is further demonstrated in Figure 4.

Of special interest is the double-value property of X_{max}, solutions in which either the wall temperature is very near the gas temperature at entry and little heat is released, on one in which the two temperatures are quite different and a great deal of reaction has occurred. For example at $\dot{V} = 6$ l/min a maximum in the temperature profile within the catalyst duct can be established at a distance of 3 cm from the inlet to the duct when $T_{SO} = 504$ K and $T_{SO} = 539$ K. However the maximum temperatures attained at the duct wall correspond to 505 K and 753 K, respectively, as can be seen from the curves in Figure 5, in which we have correlated the maximum surface temperatures in the duct with the inlet surface temperatures. These two steady-states may be the result of two reaction regimes, one a predominantly surface-catalyzed reaction with limited heat release rate, and the other a surface initiated gas-phase reaction with high heat release rate.

As expected this increase in heat release rate is reflected in the fuel composition profiles obtained at several inlet surface temperatures (Figure 6). Again we note the significant reduction in the fraction of residual fuel as we increase the value of T_{SO}.

We have attempted to correlate the numerical results with the experimental data of the preceding Technical Report No. 2. In Figures 2 and 3 we show the experimental temperatures measured in the catalytic monolith at two inlet gas velocities. In fitting the experimental data to the theoretical curves we obtain a "best fit" on reducing the pre-exponential factor in the Arrhenius equation for the surface catalyzed

reaction by a factor of 10^{-4} from that given in Table 1. The value of $\bar{k}_s$ listed was obtained in separate experiments employing a Pt-ribbon rather than the type of wall coating with dispersed Pt on an insulator support employed in the current study. Most likely the catalyst in the monolith had lost some of the activity because of surface contaminants introduced during its preparation or during the course of experimentation on exposure to feed gas (propane and air) of modes or unknown purity. No attempt was made to "clean" the catalytic surface preceding an experiment. It is of interest that little change in activity was detectable over the course of this experimental study.

Using the reduced value for catalyst activity, we observe a satisfactory correlation between experimental results and numerical data. We conclude that the gas-phase reaction initiated by the surface-catalyzed reaction makes a significant contribution to the overall combustion process. By this mode of operation in a catalytic duct the heat release rate can be greatly augmented and the reactor volume considerably reduced. As a result of the homogeneous and heterogeneous reactions, the high heat release rates can provide a suitable source for flame holding in an afterburner.

REFERENCES

1. J. Votruba, J. Senkule, V. Hlavacek, and J. Skrivanek, "Heat and Mass Transfer in Monolithic Honeycomb Catalysts-I," Chem. Eng. Sci. Vol. 30, pp. 117-123 (1975).

2. L. L. Hegedus, "Temperature Excursions in Catalytic Monoliths" AIChE J. Vol. 21, pp. 849-853 (1975).

3. L. C. Young, B. A. Finlayson, "Mathematical Models of the Monolith Catalytic Converter," AIChE J. Vol. 22, pp. 331-353 (1976).

4. R. H. Heck, J. Wei, and J. K. Katzer, "Mathematical Modeling of Monolythic Catalyts" AIChE J., Vol. 22, pp. 477-484 (1976).

5. C. M. Ablow and H. Wise, "Contribution of Catalytic Wall Reaction to Combustion Initiation," paper 77-39, Fall Meeting, Western States Section/The Combustion Institute, Stanford, California (1977).

6. C. M. Ablow and H. Wise, "Theoretical Analysis of Catlaytic Combustion in a Monolith Reactor," Combustion Sci. and Tech. (in press).

7. C. M. Ablow, B. J. Wood,and H. Wise, "Gas-Phase Reaction in a Catalytic Monolith Combustor," Scientific Report, AFOSR Contract No. F49620-77-C-0123 (1979).

Table 1

CONSTANTS AND FUNCTION COEFFICIENTS
AVERAGE ABOUT T = 600 K

(for the experimental conditions of Figure 1)

ΔT_A = 358 K

St = $2.18/\dot{V}$

R_H = 0.0363 cm

Le = 1.0

$Pe_h = 0.225\ \dot{V}^2$

$Pe_W = 0.0031\ \dot{V}^2$

$\bar{k}_S = 8.67 \times 10^7 \exp(-8500/T_S)$

$\bar{k}_G = 2.15 \times 10^5 \exp(-10500/T_G)$

T_{GO} = 500 K

N_W = 0

L = 15 cm

In the above $\dot{V}$ has the units ($l \cdot min^{-1}$) and T(K).

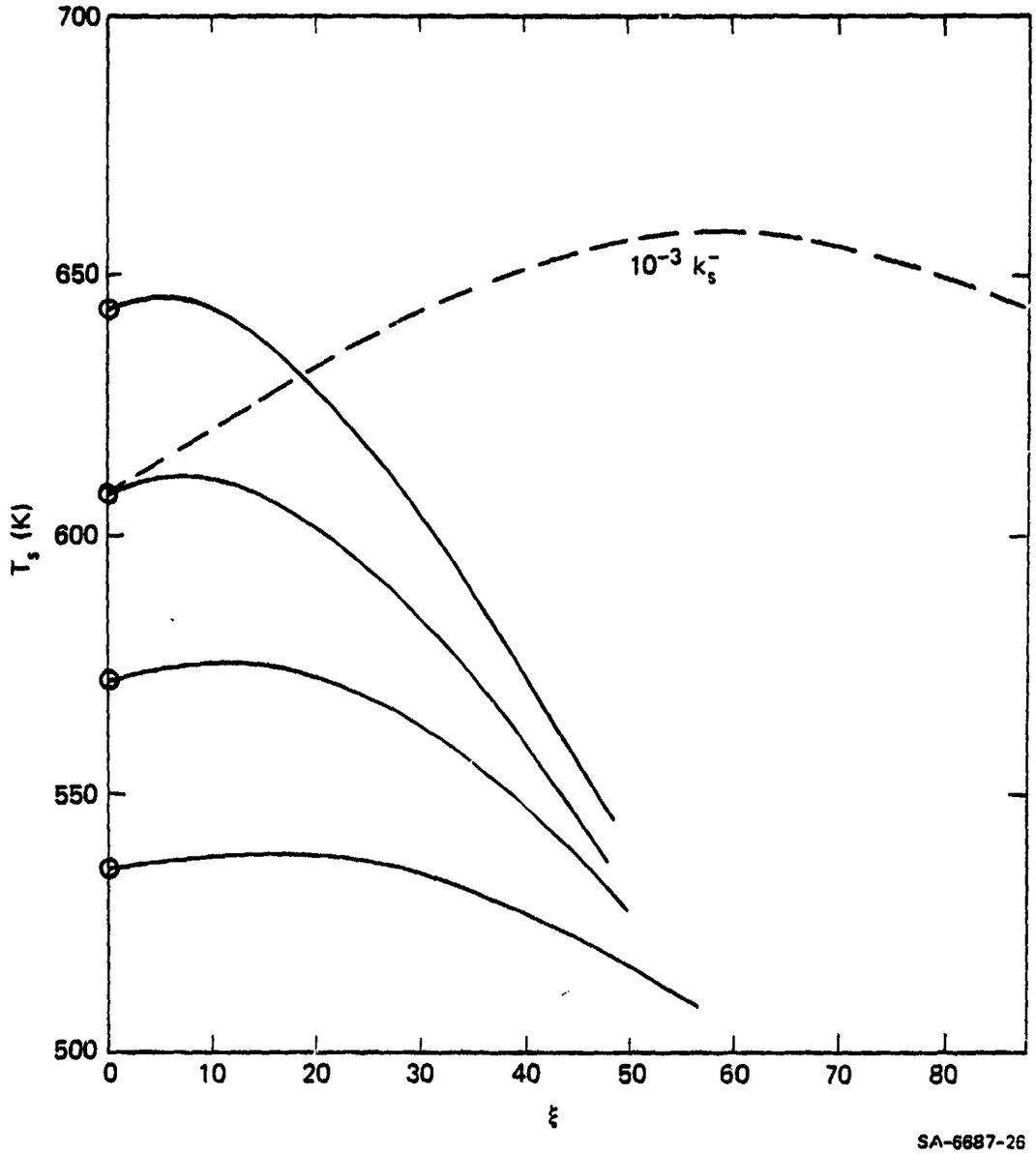

FIGURE 1 TEMPERATURE PROFILE IN CATALYTIC MONOLITH DUCT

[Inlet: gas temperature = 500 K, 0.5 vol. % C_3H_8 in air; surface rate constant $k_s^- = 8.67 \times 10^4 \exp(-8500/T_s)$; $k_g^- = 2.15 \times 10^5 \exp(-10500/T_G)$; $\dot{V} = 2\ell$/min]

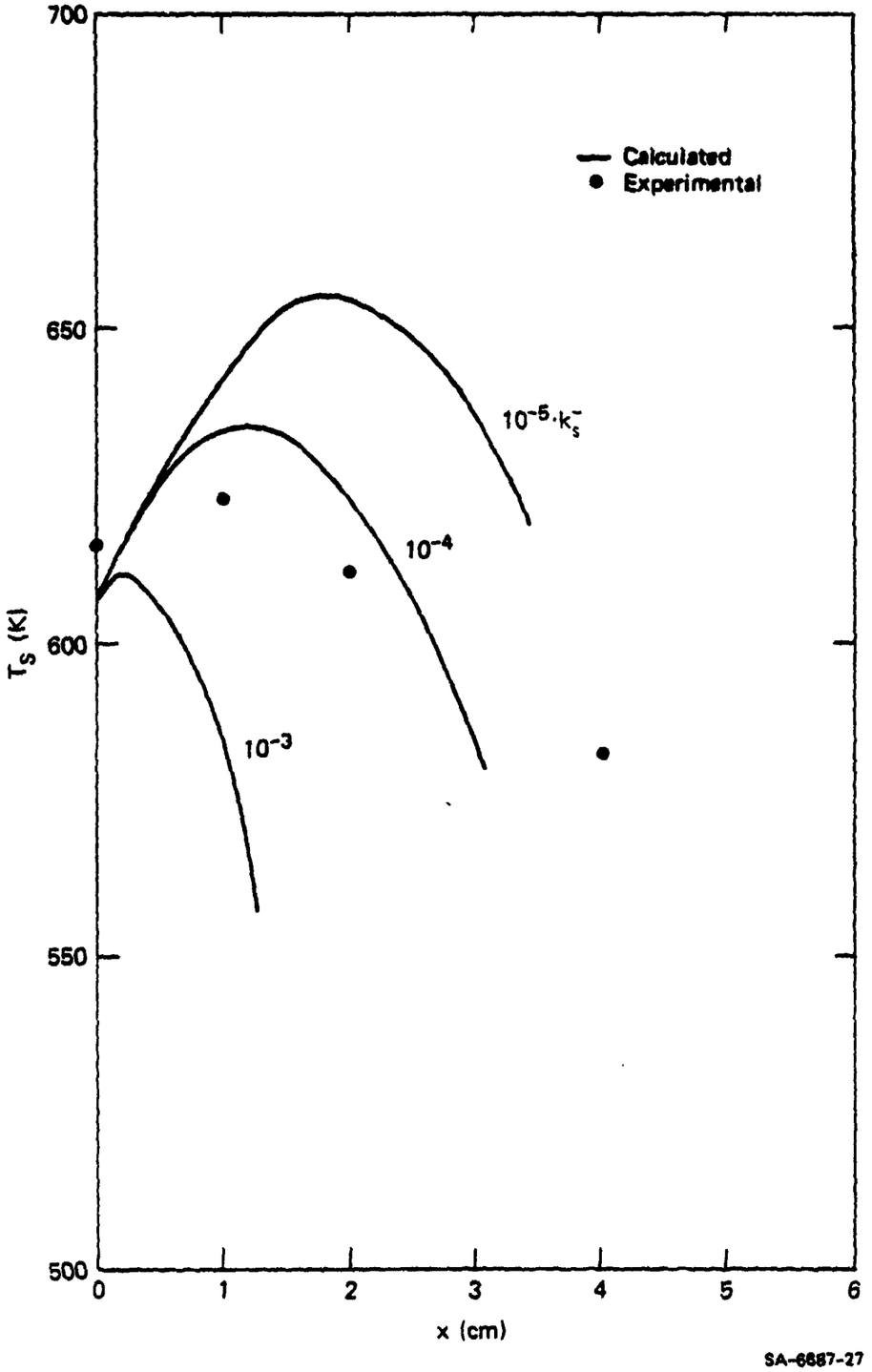

FIGURE 2 EFFECT OF SURFACE REACTIVITY ON TEMPERATURE PROFILE IN CATALYTIC MONOLITH DUCT

[Inlet: gas temperature = 500 K, 0.5 vol. % C_3H_8 in air; $k_g^- = 2.15 \times 10^5 \exp(-10{,}500\ T_G)$; $k_s^- = 8.6 \times 10^7 \exp(-8500/T_S)$; $\dot{V} = 2\ell$/min]

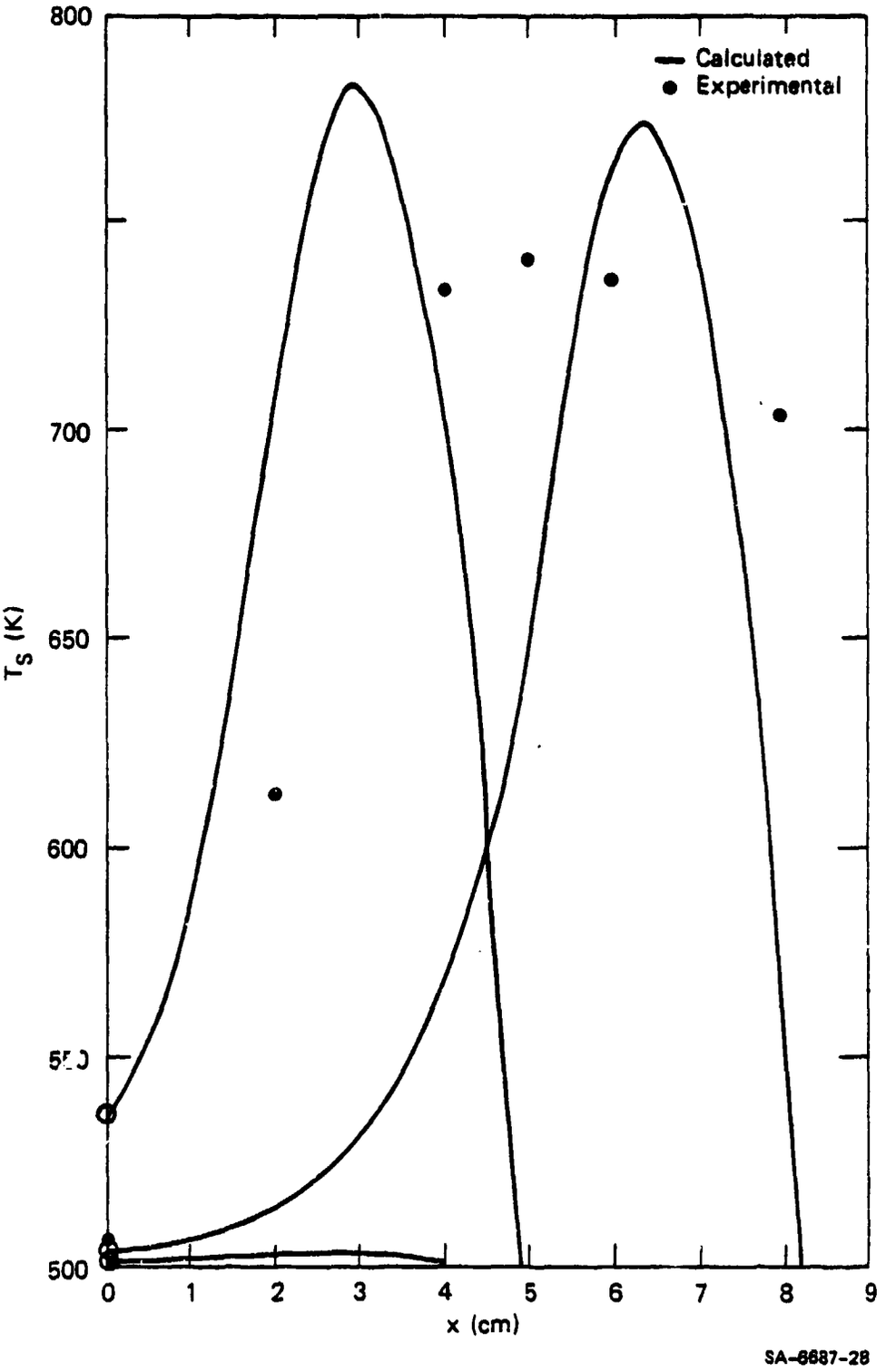

FIGURE 3 TEMPERATURE PROFILE IN CATALYTIC MONOLITH DUCT

Inlet: Gas temperature = 500K; 0.5 vol % C_3H_8 in air; $k_g^- = 8.67 \times 10^3 \exp(-8500/T_S)$; $\dot{V} = 6\ell/\text{min}$]

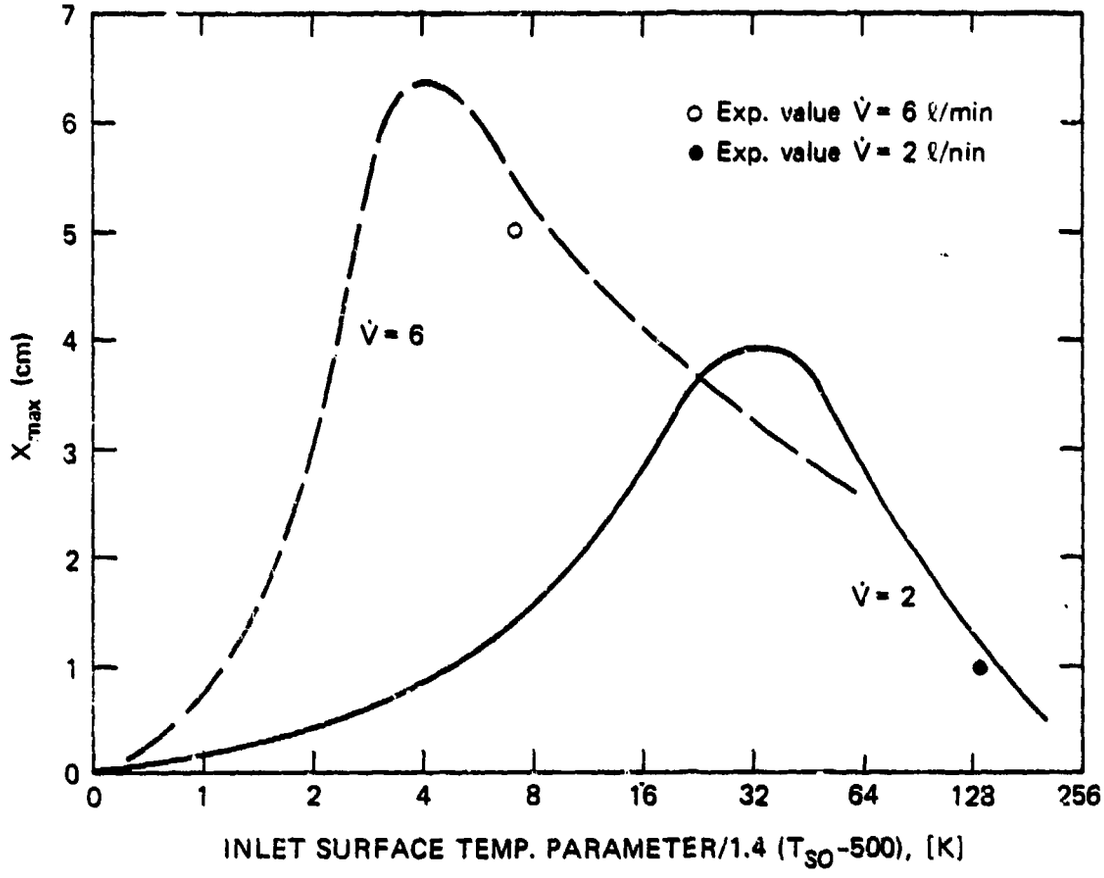

FIGURE 4 LOCATION OF TEMPERATURE MAXIMUM X_{max} IN CATALYTIC MONOLITH DUCT AT DIFFERENT GAS VELOCITIES

[Inlet: gas temperature = 500 K; 0.5 vol. % C_3H_8 in air; $k_g^- = 2.15 \times 10^5 \exp(-10{,}500/T_G)$; $k_s^- = 8.67 \times 10^3 \exp(-8500/T_S)$]

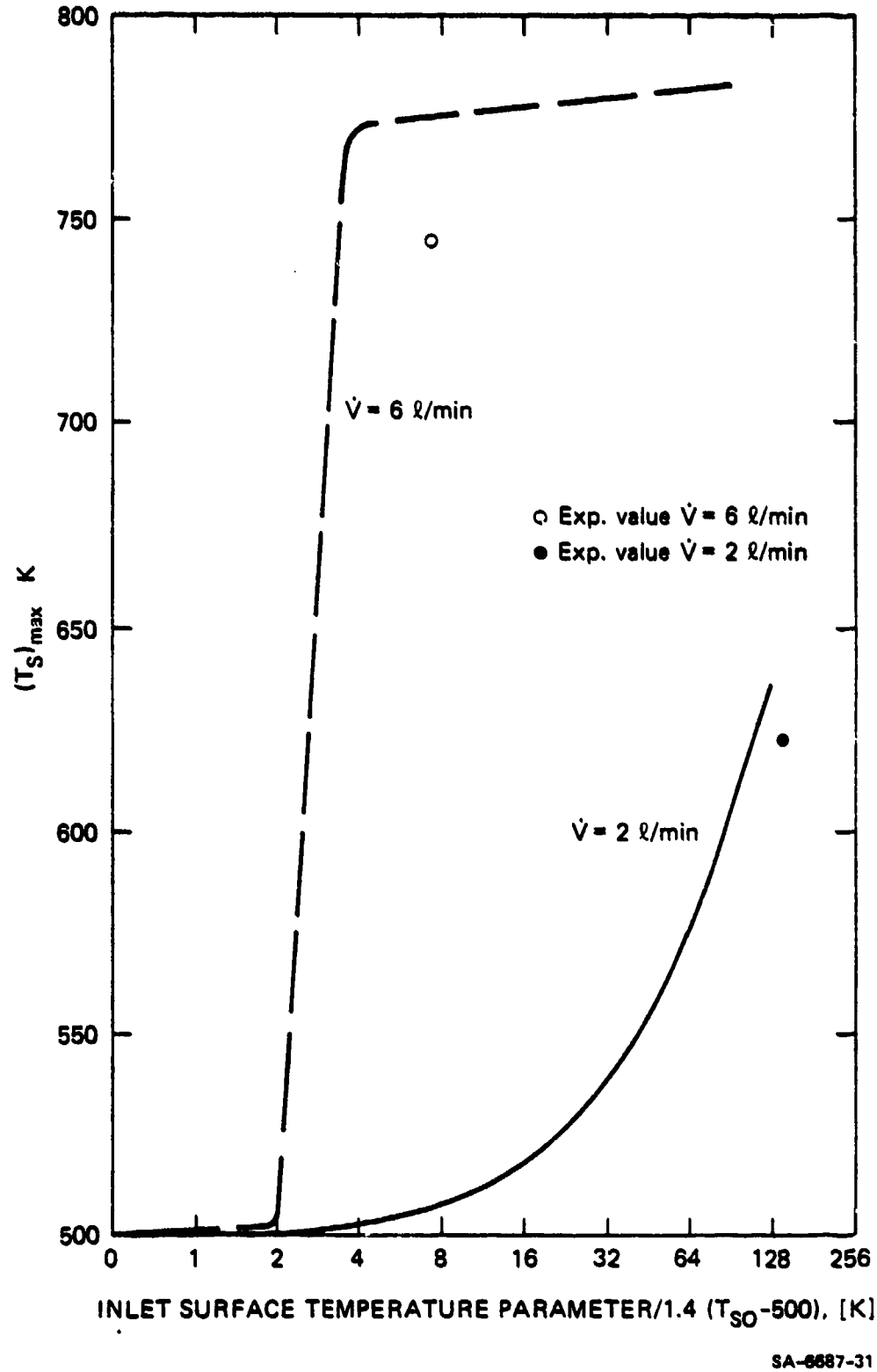

FIGURE 5 MAXIMUM TEMPERATURE IN CATALYTIC MONOLITH DUCT AT VARIOUS INLET SURFACE TEMPERATURES AND GAS VELOCITIES

[Inlet gas temperature = 500 K; 0.5 vol. % C_3H_8 in air; $k_g^- = 2.15 \times 10^5 \exp(-10{,}500/T_G)$; $k_s^- = 8.67 \times 10^3 \exp(-8500/T_S)$]

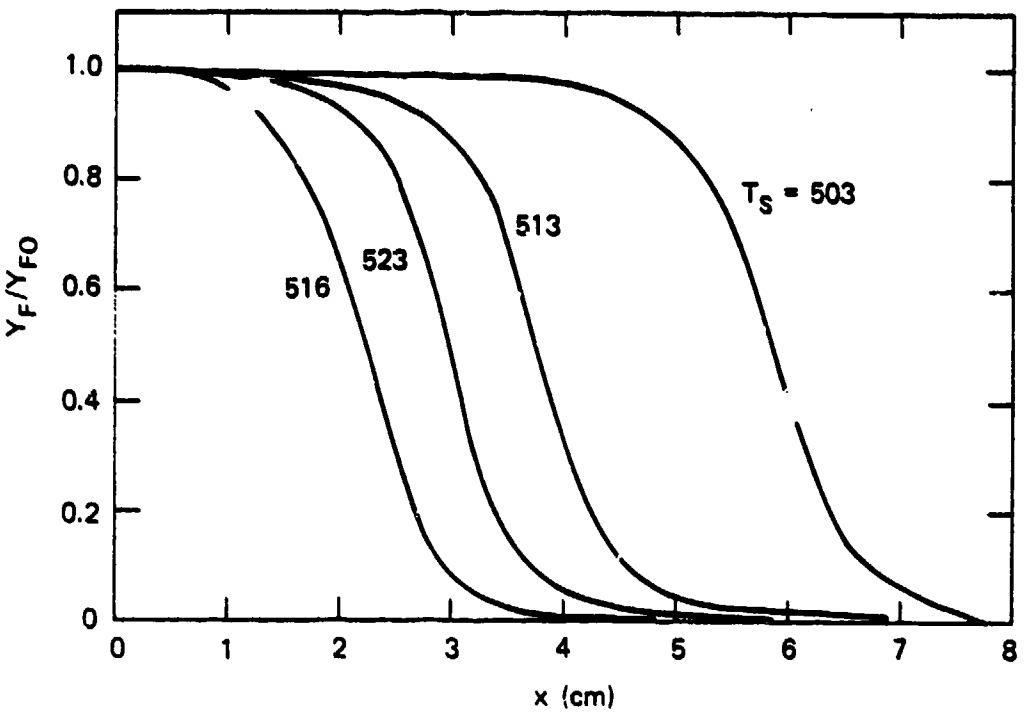

FIGURE 6 RESIDUAL FUEL FRACTION IN CATALYTIC MONOLITH DUCT AT DIFFERENT FUEL SURFACE TEMPERATURES

(Gas inlet temp. = 500 K; 0.5 vol. % C_3H_8 in air, gas flow 6ℓ/min; k_g^- and k_s^- same as in Figures 4 and 5)